CANADIAN JOURNAL OF RESEARCH

VOLUME 25 JANUARY, 1947 NUMBER 1

— SECTION A —

PHYSICAL SCIENCES

Contents

NATIONAL RESEARCH COUNCIL
OTTAWA, CANADA

CANADIAN JOURNAL OF RESEARCH

The *Canadian Journal of Research* is issued in six sections, as follows:

A. Physical Sciences	D. Zoological Sciences
B. Chemical Sciences	E. Medical Sciences
C. Botanical Sciences	F. Technology

For the present, each of these sections is to be issued six times annually, under separate cover, with separate pagination.

The *Canadian Journal of Research* is published by the National Research Council of Canada under authority of the Chairman of the Committee of the Privy Council on Scientific and Industrial Research. The *Canadian Journal of Research* is edited by a joint Editorial Board consisting of members of the National Research Council of Canada, the Royal Society of Canada, and the Chemical Institute of Canada.

Sections B and F of the *Canadian Journal of Research* have been chosen by the Chemical Institute of Canada as its medium of publication for scientific papers.

Manuscripts should be addressed:

Editor-in-Chief,
Canadian Journal of Research,
National Research Council, Ottawa, Canada.

Canadian Journal of Research

Issued by THE NATIONAL RESEARCH COUNCIL OF CANADA

VOL. 25, SEC. A. JANUARY, 1947 NUMBER 1

A MASS SPECTROMETER INVESTIGATION OF THE ISOTOPES OF XENON AND KRYPTON RESULTING FROM THE FISSION OF U^{235} BY THERMAL NEUTRONS[1]

BY H. G. THODE[2] AND R. L. GRAHAM[3]

Abstract

Mass spectrometer investigations have been made of rare gas fission products extracted from uranium irradiated with thermal neutrons. The irradiated uranium rods were allowed to stand for various periods of time after irradiation to permit the decay of most fission product chains to stable isotopes. Four stable isotopes of xenon were found having mass numbers 131, 132, 134, and 136, and three stable isotopes of krypton with mass numbers 83, 84, and 86. Kr^{86}, the most abundant of the latter group, is probably formed directly in fission. In addition a long lived krypton with mass 85 was discovered which is isomeric with a 4.0 hr. Kr^{85} reported previously.

The relative abundances of these isotopes which are related directly to fission yields of the corresponding mass chains have been determined with an accuracy of 1% or better. The mass numbers of these fission chains can now be identified with certainty by comparing mass spectrometer abundance data with known yield values of the active chain members. Finally, the half-life of krypton 85 was determined by comparing its concentration to that of a stable isotope over a period of time.

Introduction

In the uranium fission process a thermal neutron is captured by the U^{235} nucleus. This gives rise to an activated compound nucleus U^{236*}, which in turn splits into two fragments or fission products in addition to several neutrons. The process can be represented by the following equation

$$U^{235} + n \longrightarrow U^{236*} \longrightarrow Z_1^{A_{m_1}} + Z_2^{B_{m_2}} + v\,(n)$$

where $Z_1 + Z_2 = 92$, and $m_1 + m_2 + vn = 236$.

The primary fission products A and B have more neutrons for their charge than the stable nuclei and undergo β-disintegrations in several steps ending in stable nuclear structures. Some 64 such fission chains are now known.†

Most of the work with fission products has involved a study of the activity of the separated active products. The difficulties involved in getting clean-cut separations of active products, in determining mass numbers of fission

[1] *Manuscript received September 24, 1946.*

Contribution from the Department of Chemistry, McMaster University, Hamilton, Ont.

[2] *Professor.*

[3] *Physicist, Division of Atomic Energy, National Research Council of Canada.*

* *The fission product work reported here was done at McMaster University, Hamilton, between December 1944 and December 1945, in connection with the Canadian atomic energy project under the National Research Council of Canada.*

† *Address by C. Coryell at nuclear chemistry symposium held by the American Chemical Society at Atlantic City (April, 1946).*

product chains, and, finally, in determining accurate fission yield data by these methods, are well known. The availability in Canada of small samples of rare gas mixtures (0.001 cc. of gas at N.T.P.) extracted from irradiated uranium for volume measurements and counting (2) experiments, made possible for the first time a mass spectrometer study of certain stable isotopes resulting from fission product chains. Because of the large number of stable isotopes of xenon and krypton which block further β-disintegration of fission product chains, the mass spectrometer experiments were expected to give important information about a relatively large number of these chains.

Some six rare gas mixtures extracted from irradiated uranium rods were investigated up to December 1945. These samples contained about 10^{-3} cc. of xenon and about 10^{-4} cc. of krypton. Altogether eight isotopes of krypton and xenon were found, seven stable and one active. Since the rods were allowed to stand for six to nine months, only long lived active isotopes will be present with the stable ones. Relative abundances of these isotopes were obtained with an accuracy of 1% or better. Details of the investigations are reported in this paper.

Experimental

Rare Gas Samples

The rare gases investigated were prepared by Drs. Arrol, Chackett, and Epstein (2), who had apparatus set up for the extraction and fractionation of rare gas mixtures for volume determinations. Details of the simple extraction are given in their papers. The uranium used was in the form of a composite rod made up of disks varying in weight. Two such rods were irradiated with neutrons in a pile. Rod 2 was irradiated at 1.5 times the neutron intensity of Rod 1, but for only two-thirds the exposure time.

Preliminary mass spectrometer investigations showed 1 cu. mm. of extracted gas to be contaminated with about 60% of argon. The 1 cu. mm. samples therefore contained less than 0.0004 cu. cm. of krypton and xenon from uranium fission. The gas sample line (see Fig. 1) was designed to handle these small samples of gas. It consists of a capillary line of 1 cc. volume leading to a capillary leak which introduces gas samples directly into the ionization chamber of the ion source system (see Fig. 2). This small volume is connected to a sample tube manifold by means of glass break seals that can be opened for pumping and for the introduction of samples. In addition, the line is fitted with a large reservoir mercury pump that is used to pump samples into the small volume behind the mass spectrometer leak. This pump is also used to mix the gas sample and to regulate the pressure of gas behind the leak, so as to obtain suitable ion currents for identification of isotopes and for abundance measurements. The small 1 cc. volume can be sealed off from the rest of the line at the second break seal manifold after the sample has been introduced into the large reservoir of the mercury pump. After the investigation of each sample, the residual gas can be condensed in a charcoal liquid air trap and stored for further work.

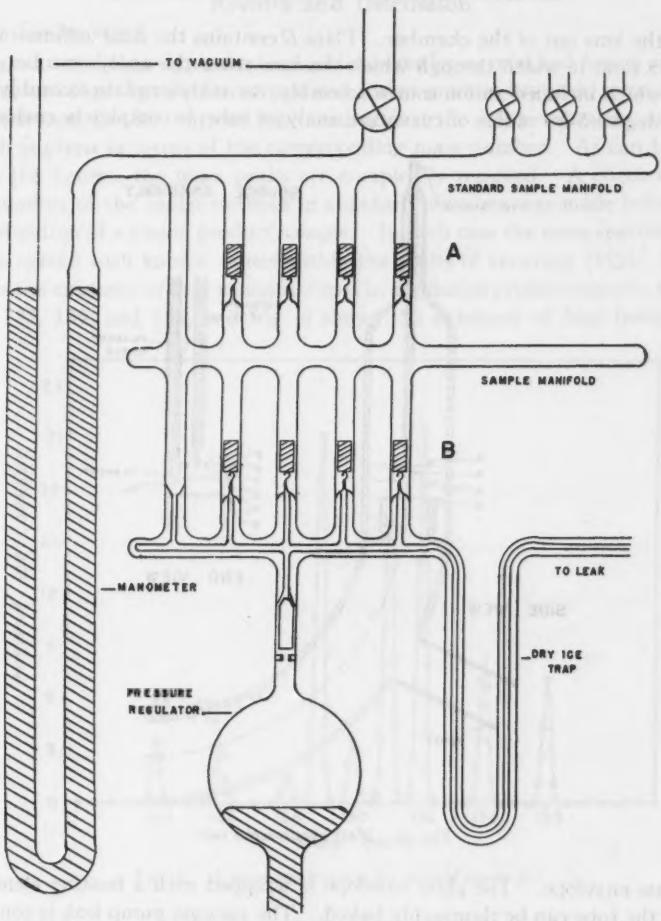

FIG. 1. *Mass spectrometer sample line for rare gas samples.*

Mass Spectrometer

The mass spectrometer used is a 180 degree Nier type described previously (6, 7, 10). The ion source system and part of analyser tube are shown in Fig. 2. Plate *A* is a supporting plate and forms the top of the ionization chamber. Plate *C* contains the first collimating slit, 8 mm. long and 0.35 mm. wide. Between Plates *A* and *C* is located a box through which electrons pass from a filament through a 0.2 mm. slit and ionization chamber to a collector box or trap, *T*. Plate *B*, mounted in the ionization chamber over the first collimating slit, is made 1 to 5 volts more positive than Plate *C*, in order to

draw the ions out of the chamber. Plate *D* contains the final collimating slit of 0.25 mm. in width through which the ions enter the analyser tube. The tube, which included an ion source assembly, an analyser plate assembly, and a 180 degree 5-in. radius of curvature analyser tube, is completely enclosed in

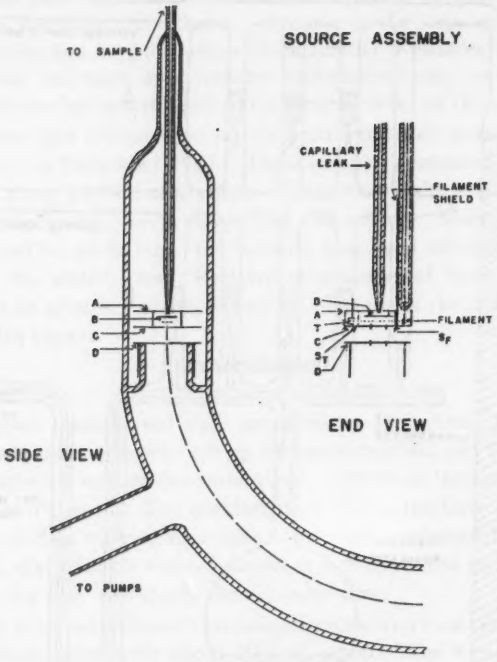

FIG. 2. *Mass spectrometer tube.*

a glass envelope. The glass envelope is wrapped with a heating element so that the tube can be thoroughly baked. The vacuum pump leak is connected directly to the analyser tube to ensure a low pressure in this region, and thereby reduce scattering of the ion beams to a minimum. With this arrangement there exists a pressure gradient between the source end and the analyser tube, which are connected by means of the slit in Plate *D*, and between the ionization chamber where the gas samples enter and the source end of the tube, since this chamber is enclosed but for two small slits.

A d-c. amplifier with linear feedback is used to measure the ion currents. This unit, in addition to the electronic equipment for control of electron emission, accelerating of ions, and stabilization of magnetic current, have been designed to operate from standard a-c. power lines. Details of these units and a discussion of their performances are described elsewhere (5).

Results and Discussion

Mass Spectrograms

Figs. 3 and 4 show typical mass spectrograms for normal and fission product xenon, and Figs. 5 and 6 for normal and fission product krypton, respectively. In each case the ion current is plotted against the ion accelerating voltage, which is given in terms of the corresponding mass number. As can be seen from the figures, the mass peaks are completely resolved. A check on the abundances of the xenon isotopes in standard mixtures was made before the investigation of a fission product sample. In each case the mass spectrometer ratios agreed with known values within the limits of accuracy (1%). Fig. 4 shows the existence of four xenon isotopes in the fission product sample, masses 131, 132, 134, and 136, and Fig. 6 shows the existence of four isotopes of

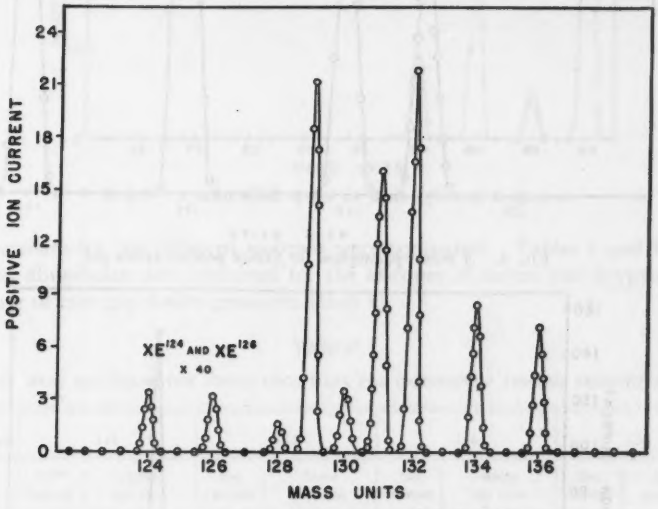

FIG. 3. *A mass spectrogram for normal xenon gas.*

krypton with masses 83, 84, 85, and 86. In the identification of these masses, all the usual precautions were taken and the possibility of contamination was investigated thoroughly. In the first sample investigated, xenon 129 was found to be present to the extent of 1 part in 2000 of the total number of xenon atoms. However, contamination with normal xenon was suspected because of the high concentration of Xe^{129} in naturally occurring xenon. Later work showed this to be the case. Contaminated samples were found to have traces of Xe^{129} and Xe^{130} in proportion to their abundances in normal xenon. Other samples free of contamination contained less than 1 part in 40,000 of these two isotopes, which is the limit of detection for the instrument with the size of samples available. The largest samples investigated showed the

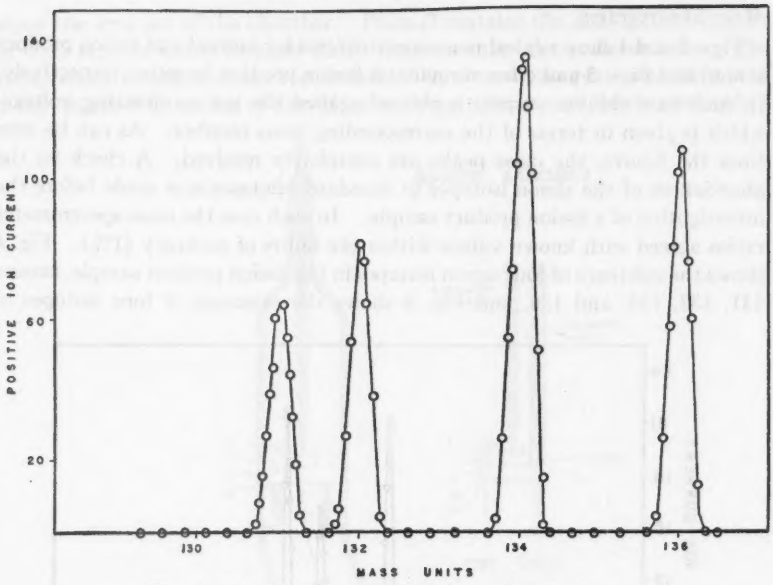

FIG. 4. *A mass spectrogram for fission product xenon gas.*

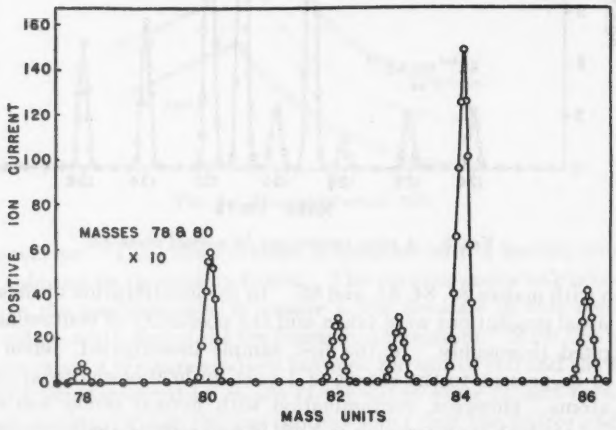

FIG. 5. *A mass spectrogram for normal krypton gas.*

existence of trace amounts of krypton 80 and 82. These traces amounted to less than 1 part in 8000 and 5000, respectively, in terms of total krypton.

Isotope Abundances and Fission Yields

The samples investigated contained only from 1×10^{-4} to 1×10^{-3} cc. of xenon and krypton. It was therefore necessary to use a very small volume

behind the mass spectrometer leak and operate at relatively low pressures. Because of this the ion currents decreased slowly with time. However, by making time corrections, quite precise abundance data were obtained. The

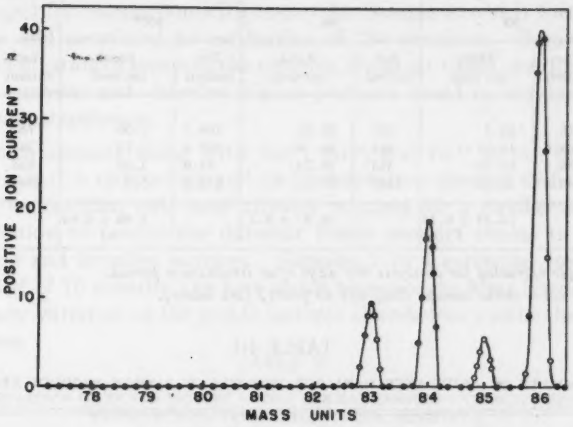

FIG. 6. *A mass spectrogram for fission product krypton.*

ion currents for the different isotopes were compared. Tables I and II give typical abundance data obtained for the isotopes of xenon and krypton in a mixture of rare gas fission products (Rod 1).

TABLE I

TYPICAL MASS SPECTROMETER ABUNDANCE DATA FOR ISOTOPES OF FISSION PRODUCT XENON*

Mass unit	131		132		134		136	
Set	Ion** current	Atom per cent	Ion current	Atom per cent	Ion current	Atom per cent	Ion current	Atom per cent
1	255	13.67	370.5	20.35	670	35.92	560	30.02
2	241	13.76	358.9	20.52	633.1	36.18	516	29.49
3	236.4	13.76	351.6	20.47	620.3	36.09	509	29.73
4	1083.6	13.75	1602.4	20.33	2838.0	36.00	2355	29.87
5	204.4	13.73	301.4	20.25	553.8	35.87	448	30.10
Average		13.73 ± 0.03		20.38 ± 0.08		36.01 ± 0.1		29.82±0.2

* *Sample extracted 407 days after the irradiation period.*

** *Ion current given in terms of galvanometer deflection in centimetres.*

Tables III and IV give a summary of stable isotope abundances obtained with five samples of rare gas mixtures. Samples 1 to 4 were extracted from the centre disk of a single uranium rod referred to as Rod 1. Sample 5 was extracted from centre disk in Rod 2, which was irradiated at $1\frac{1}{2}$ times the

TABLE II

TYPICAL MASS SPECTROMETER ABUNDANCE DATA FOR ISOTOPES OF FISSION PRODUCT KRYPTON*

Mass unit	83		84		85**		86	
Set	Ion current	Atom per cent	Ion current	Atom per cent	Ion current	Atom per cent	Ion current	Atom per cent
1	215	14.3	401	26.61	106.2	7.06	781	51.90
2	204.6	14.25	383	26.70	102.5	7.13	744	51.75
3	186.5	14.10	353	26.75	93.0	7.06	686	52.0
4	540.0	13.82	1067	27.2	273.5	7.0	2026	51.8
Average		14.12 ± 0.15		26.81 ± 0.2		7.06 ± 0.04		51.86 ± 0.08

* *Sample extracted for analysis 407 days after irradiation period.*
** *Kr^{85} not a stable isotope (half-life 10 years) (see below).*

TABLE III

SUMMARY OF ABUNDANCE DATA FOR ISOTOPES OF FISSION PRODUCT XENON

Sample	Mass unit			
	131	132	134	136
1 (Rod 1)	13.9 ± 0.1	20.4 ± 0.1	36.0 ± 0.1	29.7 ± 0.1
2	13.7 ± 0.1	20.25 ± 0.1	36.0 ± 0.1	30.1 ± 0.1
3	13.68 ± 0.04	20.45 ± 0.03	36.05 ± 0.06	29.84 ± 0.03
4	13.73 ± 0.03	20.38 ± 0.08	36.01 ± 0.1	29.82 ± 0.2
Average	13.73 ± 0.04	20.37 ± 0.05	36.04 ± 0.04	29.86 ± 0.09
1 (Rod 2)*	13.38 ± 0.04	20.09 ± 0.04	35.76 ± 0.04	30.77 ± 0.04

* *Rod 2 was irradiated at 1.5 times the neutron intensity of Rod 1 but only for two-thirds of the exposure time.*

TABLE IV

SUMMARY OF ABUNDANCE DATA FOR STABLE ISOTOPES OF FISSION PRODUCT KRYPTON*

Sample	Mass unit		
	83	84	86
1 (Rod 1)	14.1	28.3	57.6
2	15.8	29.2	55.0
3	15.1	28.7	56.2
Average (1-3)	15.0 ± 0.5	28.7 ± 0.3	56.3 ± 1.2
4 (Rod 1)	15.23 ± 0.15	28.90 ± 0.2	55.87 ± 0.1
1 (Rod 2)	15.39 ± 0.05	28.91 ± 0.05	55.70 ± 0.05

* *Active krypton 85 not included since its concentration is a function of time and would vary from sample to sample.*

neutron density for two-thirds as long an irradiation time. The first three samples contained such small amounts of krypton that it was difficult to estimate the precision of the abundance data. These three sets of data have been averaged for comparison with results for Sample 4, which was considerably larger and permitted an estimation of the precision. Because of the higher concentration of xenon in the samples, about six times that for krypton, higher ion currents and therefore higher precision could be obtained for the xenon isotope abundances.

Kr^{85}, which appears along with Kr^{83}, Kr^{84}, and Kr^{86}, is not included in Table IV since it is radioactive and its concentration changes with time. In each case the uranium rods were allowed to stand for a number of months after irradiation to permit the different fission product chains to decay to stable xenon and krypton isotopes. Samples 1 to 4 extracted from Rod 1 over a period of 10 months, the first about nine months after irradiation, do not show any variation in the stable isotopic abundances within the limits of our precision.

TABLE V

COMPARISON OF XENON ISOTOPE RATIOS FOR GAS SAMPLES EXTRACTED FROM URANIUM RODS IRRADIATED UNDER SLIGHTLY DIFFERENT POWER CONDITIONS

Rod No.	Mass ratio		
	132/131	134/131	136/131
1	1.48	2.63	2.17
2	1.50	2.67	2.30
Difference, %	1.3	1.5	6.0

TABLE VI

COMPARISON OF KRYPTON ISOTOPE RATIOS FOR GAS SAMPLES EXTRACTED FROM URANIUM RODS IRRADIATED UNDER SLIGHTLY DIFFERENT POWER CONDITIONS

Rod No.	Mass ratio	
	84/83	86/83
1	1.90	3.66
2	1.88	3.62
Difference, %	1.0	1.1

In Tables V and VI, the stable isotopic ratios for fission product xenon and krypton obtained for Rods 1 and 2 are compared. These results show that stable krypton isotope ratios for the two agree well within the limits of our precision, but that the xenon isotope ratios differ for the two by as much as

6%. It would appear that even the small variations in the 132/131 and 134/131 ratios are significant, in view of the high internal precision of the measurements. Certainly the large difference in the 136/131 ratio is significant and cannot be explained on the basis of mass discriminations in the mass spectrometer. If this explanation were true, larger discrepancies would have shown up for the krypton isotope ratios, which were examined at the same time. Further, the variations indicated in Table V are not a linear function of the masses.

Krypton 85

Ion currents appeared corresponding to mass 85 in all krypton fission product samples. Purification of the krypton samples did not alter the results of relative abundance measurements and there was no evidence for contamination in the mass spectrometer tube or the sample line that could give rise to a mass 85 ion current. A number of samples have been investigated and it is now quite clear that Kr^{85} is a product of the fission process and is radioactive with a half-life of about 10 years.

The discovery of this isotope was a little surprising in view of the existence of a four hour Kr^{85} reported previously. The new isotope is obviously an isomer of the four hour Kr^{85} with a long half-life. A sample of krypton extracted from a uranium rod 407 days after its irradiation with neutrons formed in a pile was found to contain $7.06 \pm 0.04\%$ of the active Kr^{85} isotope (see Table II). This concentration was found to be less in older samples and greater in younger samples, indicating a definite activity. This activity was also investigated by Arrol, Chackett, and Epstein, who pumped fission product krypton into a gas counter (3). Recently the existence of a long lived krypton isotope was mentioned in an address by C. Coryell†, its discovery being attributed to N. Sugarman and C. Hoagland. Undoubtedly, this isotope, found independently by counting experiments, is the active Kr^{85} positively identified by mass spectrometer methods.

The decrease in the Kr^{85} concentration with time relative to one or more of the stable krypton isotopes was measured and its half-life calculated. The results are given in Table VII. In these calculations the assumption is made that variations in the Kr^{85} concentration relative to the stable isotopes from sample to sample are due wholly to the decay of Kr^{85} with time, and not due to variations in the distribution of fission product isotopes. This assumption seems justified for the first two calculations made, Rows 1 and 2, Table VII, since the samples investigated were extracted in each case from the centre disks of the same uranium rods, and the relative abundance measurements did not show any significant variations in the distribution of the stable isotopes of krypton and xenon that result from fission. The third calculation made from data in Row 3, Table VII, is perhaps less justified since the 144 day sample came from a uranium rod different from that of the 407 day one, and the relative abundance measurements for the two samples did show signifi-

†*See footnote, page 1.*

TABLE VII

Kr^{85} HALF-LIFE FROM MASS SPECTROMETER ABUNDANCE DATA

Ratio	Time after irradiation, days			Kr^{85} half-life calculated, years
	144	407	619	
Stable Kr^{86}/active Kr^{85}	—	7.35	7.6	11
Stable Kr^{84}/active Kr^{85}	—	3.80	3.96	9
$\frac{\text{Stable } Kr^{83} + {}^{84} + {}^{86}}{\text{Active } Kr^{85}}$	12.44*	13.16	—	9

* *This sample from uranium rod No. 2, all others from rod No. 1.*

cant variations in the Xe^{136} concentration. However, the variations in the relative concentrations of the other stable isotopes of xenon and krypton were small and perhaps not significant.

The results of the three half-life calculations agree fairly well, considering the small changes in the Kr^{85} concentration measured. The assumptions made in above calculations become unnecessary when abundance measurements can be made on the same sample of rare gas. A larger sample, which will be sufficient for several investigations, and which can be studied over many months, is therefore being prepared.

The fission yield of the 10 year Kr^{85} can be calculated in terms of Kr^{83} from the data in Table II. Considering the half-life to be 10 years and the sample 407 days old, the ratio of 84/85 turns out to be 3.50.

Ratio of Xenon to Krypton

To date it has been difficult to determine with high accuracy the ratio of total xenon to total krypton with the mass spectrometer, because of the small size of the rare gas samples available and the difficulties encountered in calibrating the instrument with standard rare gas samples of that size. It was found that, under the conditions necessary to handle these small samples, there was considerable fractionation of the sample at the capillary leak. However, by extensive calibration of the instrument with small standard rare gas mixtures, a preliminary value of 6.2 has been obtained for the ratio of xenon to krypton. This compares with 5.0 obtained by Arrol, Chackett, and Epstein (2), who fractionated rare gas fission product mixtures and measured the volumes of the different components. A knowledge of this ratio together with the isotopic abundances makes it possible to tie in fission yield data for mass chains ending in xenon of the heavy fission product group with those ending in krypton in the light group.

Discussion

The relative abundances of the stable isotopes found in fission material give the relative fission yields of the different mass chains directly. In view of the direct character and accuracy of the measurements, these fission yield

values should make it possible to draw the fission yield–mass number curve with greater certainty. Actually fission yield data obtained by counting experiments is only good to ± 10%. From a knowledge of the absolute fission yield of the 131 mass chain obtained for the 8 day I^{131}, fission yields for mass chains 132, 134, 136, and 83, 84, 86, follow directly from our data. This would give seven points on the curve. Actually these points have been fitted to the best available curve†, and, with the exception of one point the values agree consistently. This one discrepancy is decidedly significant and indicates some sort of branching from one mass chain to another. The problem is being investigated further.

The following series compiled from Seaborg's table of isotopes may lead to stable xenon (8).

							Early branching ratio data (1)
(1)	Sb^{129}	$\xrightarrow{\beta}$	Te^{129}	$\xrightarrow{\beta}$			0.34
	4.2 hr.		32 days 72 min.				
(2)			Te^{131}	$\xrightarrow{\beta}$	I^{131}	$\xrightarrow{\beta}$ Xe^{131}	1.6
			30 min.		8 days	Stable	
(3)	Sb^{132}	$\xrightarrow{\beta}$	Te^{132}?	$\xrightarrow{\beta}$	I^{132}?	$\xrightarrow{\beta}$ Xe^{132}	5.2
	5 min.		77 hr.		2.4 hr.	Stable	
(4)	Sb^{134}	$\xrightarrow{\beta}$	Te^{134}?	$\xrightarrow{\beta}$	I^{134}?	$\xrightarrow{\beta}$ Xe^{134}?	12
	10 min.		43 min.		54 min.	Stable	
(5)					I	$\xrightarrow{\beta}$ Xe^{-}	
					1.8 min.		

Seaborg in his 1944 table of isotopes refers to the mass numbers for 3 and 4 as > 131. Since only four isotopes of xenon have been identified with the mass spectrometer, and Xe^{131} is definitely associated with the eight day I^{131}, the Xe^{132}, Xe^{134}, Xe^{136}, must be associated with the series 3, 4, and 5 above, respectively. The order seems fairly certain, since one might expect the iodines to become less stable with increasing mass. Further fission yield data reported for the above series should agree with the relative abundances obtained for the corresponding xenon isotopes, and in this way the mass numbers can be assigned to the various series with certainty.

Xe^{129}, as mentioned above, does not exist in fission product xenon within detection limits 1 part in 40,000. On the other hand, the fission yield of the 129 series determined from the activities of Sb and Te (Anderson, Fermi, and Grosse (1)) is 0.34%. This suggests the existence of a long lived I^{129}, which

†*See footnote, page 1.*

has been suspected for some time since no activity that could be attributed to I^{129} has yet been found.

The following fission product chains previously indicated (8) might give rise to stable Kr.

(1) Br^{83} —β decay→ Kr^{83}
140 min. Stable

(2) Br^{84} —β→ Kr^{84}
30 min. Stable

(3) Br^{85} —β→ Kr^{85}
3 min. 4 hr.

(4) Br^{87}? —β→ Kr^{87}?
50 sec.

From the mass spectrometer results, we can conclude that only four stable isotopes of krypton exist in fission material in more than trace amounts, Kr^{83}, Kr^{84}, Kr^{85}, and Kr^{86}. The presence of Kr^{83} and Kr^{84} was expected since the mass numbers for Series 1 and 2 above had been definitely established previously by $Se(d, n)Br^{83}$ and $Rb(n, \alpha)Br^{84}$ reactions, respectively (4, 9). However, no previous mention had been made of the possible production of Kr^{86}, and Kr^{85} was entirely unsuspected in view of the known four hour Kr^{85}, which would have completely decayed in the 10 month period that elapsed between the time of irradiation and analysis. The assignment of mass number 85 to Series 3 is considered certain by Seaborg (8). The Kr^{85} discovered with the mass spectrometer must therefore be an isomer of the four hour Kr^{85} with a long half-life. This conclusion led to the half-life determinations given in Table VII. Further counting experiments of Arrol, Chackett, and Epstein on fission product krypton gas revealed an active krypton with a long period (3).

There is no known evidence for Br^{86}, which would be a parent to Kr^{86}. Therefore either the parent of Kr^{86} has a very short half-life and has escaped detection, or Kr^{86} is formed directly in fission, or both.

The mass spectrometer method is particularly suited to the study of fission products. It is the only method that gives information about the stable isotopes that grow from active products and that may form directly in fission. Mass numbers can be positively identified and relative fission yield data for the stable isotopes give a good deal of information about chain relations and possible decay mechanisms. Further, active products with long half-lives can be investigated and their periods determined. By extracting fission product samples from irradiated uranium soon after irradiation, the method can be extended to the short period isotopes as well. It is planned to explore this method further with the investigation of active rare gas samples. It will be of considerable interest also to follow changes in the relative abundances

of the different fission product isotopes as a function of time after irradiation and as a function of the pile irradiation intensity. Indications are that significant variations occur in the distribution of fission products, depending on the intensity of irradiation (see Table V). Further, the accurate mass spectrometer determination of the krypton isotope abundances furnishes a very sensitive method for detecting changes in fission product distribution effected by changes in the energy of neutrons in the irradiation process, since the krypton isotopes fall on the steep part of the fission yield–mass curve.

References

1. ANDERSON, H. L., FERMI, E., and GROSSE, A. V. Phys. Rev. 59 : 52-56. 1941.
2. ARROL, W. J., CHACKETT, K. F., and EPSTEIN, S. Private communication.
3. ARROL, W. J., CHACKETT, K. F., and EPSTEIN, S. Unpublished work.
4. BORN, H. J. and SEELMANN-EGGEBERT, W. Naturwissenschaften, 31 : 420. 1943.
5. GRAHAM, R. L., HARKNESS, A. L., and THODE, H. G. J. Sci. Instruments. In press.
6. NIER, A. O. Phys. Rev. 52 : 933-937. 1937.
7. NIER, A. O. Rev. Sci. Instruments, 11 : 212-216. 1940.
8. SEABORG, G. T. Rev. Modern Phys. 16 : 1-32. 1944.
9. SNELL, A. H. Phys. Rev. 52 : 1007-1022. 1937.
10. THODE, H. G., GRAHAM, R. L., and ZIEGLER, J. A. Can. J. Research, B, 23 : 40-47. 1945.

MEASUREMENT OF THE DIFFUSION LENGTH OF THERMAL NEUTRONS IN GRAPHITE[1]

By H. G. Hereward[2], G. C. Laurence[3], H. R. Paneth[2], and B. W. Sargent[3]

Abstract

The theory and method of measuring the diffusion length of thermal neutrons in graphite are discussed in detail. The graphite pile was a rectangular parallelepiped, 185.8 cm. square and 153.6 cm. high. The source was 1.2 gm. of radium mixed with beryllium. Part of the pile was used to slow down the neutrons to thermal velocities, and the density distribution of thermal neutrons was explored in the remainder of the pile with detectors of dysprosium oxide. The diffusion length of thermal neutrons in this graphite of average pile density 1.55 gm. per cc. was found to be 51 cm., with a probable error of 3 cm.

Introduction

The diffusion length of graphite is required in the design of graphite–uranium piles, reflectors, and thermal columns. It has also been used as an index of the purity of commercial graphites. In the early work leading up to chain reacting piles of the heterogeneous graphite–uranium type it was clear that only with some difficulty could the value of the multiplication constant k be brought above unity and the neutron density in the pile be made to diverge. Of the various steps taken to increase k, one was to increase the thermal utilization, one of the factors making up k. This was brought about by improving the purities of the uranium metal and the graphite moderator, thus minimizing the parasitic capture of thermal neutrons (see Smyth report (4)).

This paper contains an account of the measurement* of the diffusion length of thermal neutrons in a commercial graphite produced in Canada. The measurements were made in the Montreal Laboratory during June and July, 1943, and the final report was issued on October 29, 1943. It will be made clear later that the accuracy of the diffusion length depends a great deal on the size of the graphite pile. As we had at that time only nine tons in which to slow down the neutrons from a mixed radium and beryllium source and to measure their diffusion length while thermal, the accuracy was somewhat disappointing.

Description of Graphite Pile

The graphite pile weighed 9.1 short tons and was built up of unplaned bars approximately 36 by 2 by 2 in., which were cross-piled as shown in Fig. 1. The rectangular parallelepiped formed by the 29 layers of 70 bars each was

[1] *Manuscript received August 22, 1946.*

Contribution from the Physics Branch, Montreal Laboratory, Atomic Energy Division, National Research Council of Canada. Issued as N.R.C. No. 1468.

[2] *Member of United Kingdom Staff.*

[3] *Physicist, National Research Council; now at the Chalk River Laboratory.*

* *We were aware at the time of this experiment that similar work had been done in the United States.*

185.8 cm. square and 153.6 cm. high. The average pile density was 1.55 gm. per cc. while the densities of 10 planed bars taken at random were found to range from 1.58 to 1.65, with the average 1.62 gm. per cc. The pile rested on cadmium sheet, 0.3 mm. thick, covered with wrapping paper, which served to define its lower boundary for thermal neutrons.

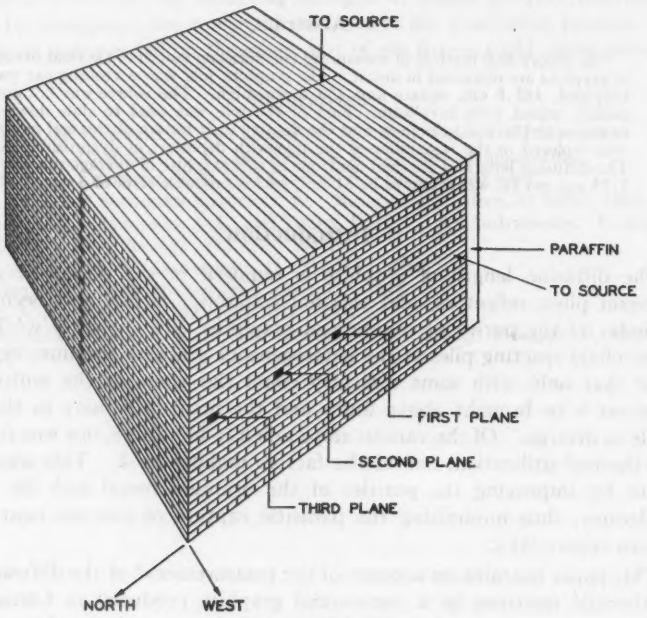

FIG. 1. *Graphite pile.*

The neutron source, 1.2 gm. of radium mixed with beryllium, was placed about 18 cm. from the south face of the pile. This face was covered with paraffin wax, about 12 cm. thick, to reduce the number of neutrons escaping from it and reaching other parts of the pile by scattering from the walls of the room.

Experimental Method

The density distribution of thermal neutrons in the pile was measured with dysprosium detectors along the central north–south axis, on which the source was placed, and in the vertical and horizontal lines that intercept this axis normally at 13.5, 50.4, and 87.2 cm. from the north face. These lines may also be described as the defining lines of three vertical east–west planes, labelled first, second, and third planes in order towards the north end of the pile. The planed movable bars into which the detectors were placed are distinguished in Fig. 1 by the shading on their ends. The perpendicular

distances from the source to the three vertical planes of measurement and the north face were 81.3, 118.1, 155.0, and 168.5 cm., respectively. This disposition of source and planes of measurement was chosen to give a volume of reasonable length (about 1.7 diffusion lengths) in which the density distribution of thermal neutrons could be explored, and at the same time to locate this volume at a sufficient distance from the source of fast neutrons that the correction for the thermal sources within it was small. The evaluation of the diffusion length therefore did not require the precise value of the slowing-down length of the neutrons from the source.

A set of 10 detectors was used. Each consisted of 280 mgm. of dysprosium oxide in a shallow aluminium tray, 23 by 11 mm. The detectors, wrapped in aluminium foil, were wedged in holes in the movable bars with half-cylindrical graphite plugs, and always faced south in the pile. In order to avoid the influence of one detector on the activity acquired by another, adjacent ones at a given time in the pile were never less than 18 cm. apart.

The relative sensitivities of the detectors were determined by exposing them in turn to neutrons under constant geometrical conditions in the pile and comparing their β-emission with that from a radium $(D + E)$ preparation. Such standards were used systematically throughout the measurements to minimize errors due to variations in the behaviour of the Geiger–Müller counters and associated amplifiers and scales-of-32.

After the activity had approximately reached saturation at a point in the pile, eight minutes from the instant of removal was allowed to elapse for short-period activity to vanish, and the dysprosium activity was compared with a radium $(D + E)$ standard by bracketing for about two hours. The density of thermal neutrons was (arbitrarily) expressed as the counting rate (β-particles per minute), corrected to saturation, at the instant of removal from the pile, taking 140 min. for the half-period of dysprosium. Corrections were also applied for any activity remaining from the previous activation, and for the long period activity (perhaps contamination) of the detector. The latter was from two to four β-particles per minute from a single detector. The half-period of dysprosium was checked to about 1% by comparing decay-curves with those of actinium active deposit, the half-period of which (36.1 min.) is accurately known.

Corrections had to be applied to the measured distribution of neutrons to allow for two extraneous effects, which would have been greatly reduced if we had had sufficient cadmium sheet and covered the pile. (i) Some neutrons entered the pile from external sources, used in other experiments in the same room. (ii) Some neutrons from the source in the pile were reflected from the walls of the room back into the pile. The contribution of these neutrons to the measurements was investigated with the dysprosium detectors by measuring the densities (*a*) at a few points in the pile in the absence of external sources, and (*b*) at many points in the pile in the presence of external sources and with our source placed in a paraffin wax box on the floor beyond the south face. In arrangement (*b*) our source was retained in the room to reproduce,

at least in part, the effect of scattered neutrons from the walls of the room. The final correction, representing the effects of all neutrons from outside the pile, of course varied from point to point in the pile but never exceeded nine β-particles per minute. When these intensities were subtracted from the original intensities, the extrapolated distributions vanished at the theoretical bounding planes for such a pile *in vacuo*.

We shall now examine our fundamental assumption that the density of thermal neutrons is proportional to the saturation activity of our detectors facing south in the pile. In order to have reasonably high counting rates we were obliged to choose rather thick detectors having a high capture cross-section per atom. When a stronger source became available, the 280 mgm. detectors, orientated in several directions, were compared with 28 mgm. detectors of dysprosium oxide at a number of points on the north–south axis of the pile. The 280 mgm. detectors acquired about 1% more activity when facing south and 1% less activity when facing north than the average for different orientations, at points between the first and third planes. The 28 mgm. detectors showed no measurable orientation effect. The ratio of the averaged activities acquired by thick and thin detectors was constant at 4.6 within experimental error. The 280 mgm. detectors, as used in this experiment, therefore give sufficiently accurate measurements of the density of thermal neutrons. A small departure from the $1/v$ law of capture of neutrons by dysprosium, suspected by some experimenters, can scarcely be of importance here.

Elementary Diffusion Theory

The diffusion equation for thermal neutrons may be simply derived from the idea of continuity in the steady state:

$$\text{production} = \text{capture} + \text{outflow},$$

$$\text{or in symbols, } q = \frac{\rho}{\tau} + \operatorname{div} j. \tag{1}$$

q is the number of thermal neutrons produced by slowing down per cm.^{3} per sec.

ρ is the density or number of thermal neutrons per cm.^{3}

τ is the mean lifetime with respect to capture.

j is the current or net number per cm.^{2} per sec.

If in analogy with the kinetic theory of gas diffusion we introduce the diffusion coefficient D and the assumption $j = -D \operatorname{grad} \rho$, the equation of continuity becomes:

$$\nabla^2\rho - \frac{\rho}{D\tau} = -\frac{q}{D}. \tag{2}$$

The product $D\tau$, having the dimensions of the square of a length, is written as L^2, where L is defined as the diffusion length. Equation (2) becomes:

$$\nabla^2\rho - \frac{\rho}{L^2} = -\frac{q\tau}{L^2}. \tag{3}$$

If we assume that there are no fast neutrons in the region beyond the first plane, which is 81.3 cm. from the source, Equation (3) becomes:

$$\nabla^2\rho - \frac{\rho}{L^2} = 0 \,. \tag{4}$$

In order to proceed to find ρ as a function of the co-ordinates, the origin is chosen at the lower north-east corner of the pile, with the positive direction of the X-axis westward, the Y-axis upward, and the Z-axis southward into the pile. The solution of the diffusion Equation (4) is subject to the boundary conditions:

$$\rho = 0 \text{ for } x = 0, a; \ \rho = 0 \text{ for } y = 0, b; \text{ and } \rho = 0 \text{ for } z = 0;$$

where $a = 189.4$ cm., $b = 157.2$ cm. are the two dimensions of the pile corrected for the breakdown of the diffusion theory near the boundaries. This correction amounts to a shift of the theoretical boundary to vacuum by a distance 0.71 times the transport mean free path. This theoretical result was brought to our attention by Placzek and Seidel's work on Milne's problem in transport theory (3) (see also Hopf (1)). The remaining boundary condition is given by the densities measured in the first plane, which may be analysed into Fourier components:

$$\rho = \sum_{l,m} K_{lm} \sin\frac{l\pi x}{a} \sin\frac{m\pi y}{b} \quad \text{at } z = d = 89 \text{ cm.}$$

where $l, m = 1, 3, 5, 7, \ldots\ldots\ldots$

The distribution is assumed to be symmetrical about the north–south axis of the pile, which was confirmed experimentally. The required solution of Equation (4) is:

$$\rho = \sum_{l,m} K_{lm} \sin\frac{l\pi x}{a} \sin\frac{m\pi y}{b} \frac{\sinh\dfrac{z}{L_{lm}}}{\sinh\dfrac{d}{L_{lm}}} \tag{5}$$

$$\text{or } \rho = \sum_{l,m} A_{lm}(z,L) \sin\frac{l\pi x}{a} \sin\frac{m\pi y}{b} \,, \tag{6}$$

$$\text{where } \frac{1}{L_{lm}^2} = \frac{1}{L^2} + \pi^2\left(\frac{l^2}{a^2} + \frac{m^2}{b^2}\right) . \tag{7}$$

The L_{lm}'s are called the relaxation lengths of the pile for the various components. The analysis of the measurements aims at isolating and evaluating L_{11} and in turn the diffusion length L through Equation (7).

Experimental Results

Fig. 2 shows the densities of thermal neutrons plotted against distances measured vertically and horizontally from the north–south axis of the pile. The density at each point was measured twice, and, taking corresponding points on opposite sides of the axis together, each density plotted in Fig. 2 is

the average of four measurements. The ordinates are the counting rates in β-particles per minute. For points in the first and second planes, where the counting rates are reasonably high, separate determinations agreed to about 3%.

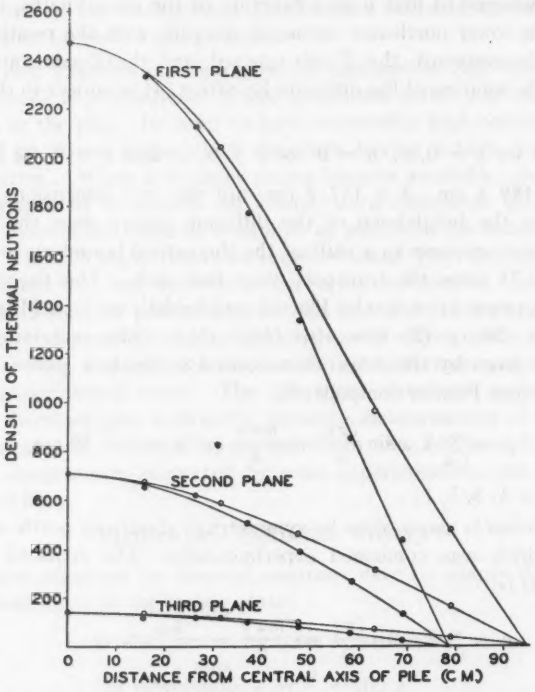

FIG. 2. *Measured densities of thermal neutrons along horizontal lines in three vertical planes are shown by unfilled circles, and those along vertical lines in the same planes are shown by filled circles. The curves shown are those for best fit according to the method of least squares.*

The amplitudes A_{lm} were found from the amplitudes of the trigonometric functions required to fit the experimental data along each axis of each plane. The method of least squares was used. Neglecting A_{33} and higher Fourier terms, the following coefficients were obtained.

First plane ($z = 89.0$ cm.)

$A_{11} = 2290$, $A_{31} = 166.5$, $A_{13} = 68.1$ ($A_{51} = -26.1$, $A_{15} = -28.4$).

Second plane ($z = 52.2$ cm.)

$A'_{11} = 673.3$, $A'_{31} = 25.7$, $A'_{13} = 9.7$ ($A'_{51} = 0.4$, $A'_{15} = -3.6$).

Third plane ($z = 15.3$ cm.)

$A''_{11} = 135.6$ ($A''_{31} = -0.1$, $A''_{13} = 0.5$).

The fit of these values is shown by the curves drawn in Fig. 2.

From Equation (5)

$$\frac{A_{11}}{A'_{11}} = \frac{2290}{673.3} = \frac{\sinh \frac{89.0}{L_{11}}}{\sinh \frac{52.2}{L_{11}}} .$$

Hence

$$L_{11} = 30.9 \text{ cm. and } L = 52 \text{ cm.}$$

Similarly,

$$\frac{A'_{11}}{A''_{11}} = \frac{673.3}{135.6} = \frac{\sinh \frac{52.2}{L_{11}}}{\sinh \frac{15.3}{L_{11}}} .$$

Hence

$$L_{11} = 31.8 \text{ cm. and } L = 57 \text{ cm.}$$

The latter values are less reliable than the former owing to the difficulty of measuring the small intensities in the third plane. A correction for thermal sources near the first plane must be applied, and this matter will be dealt with in the next section.

The densities measured along the central north–south axis of the pile are shown in Fig. 3. Each point represents the average of at least two measurements. A few points were remeasured later with a stronger source, and these results are distinguished by filled circles. These activities, averaged for different orientations of the detectors, were normalized to fit the earlier measurements at the first point. The curves were calculated for $L = 48, 52,$ and 56 cm. and a slowing-down length of 20.8 cm.

Corrections for Sources of Thermal Neutrons

Consideration of the effect of thermal sources on the derived diffusion length will be based on the slowing-down theory. It is convenient to divide the discussion into three parts.

(1) *Effect of the Paraffin Wax at the South Face*

The wax did not increase the number of epithermal neutrons beyond the first plane of measurement to any extent, for the total distance from the radium source to the wax and back to the first plane is 117 cm. or more than five slowing-down lengths. The wax may have increased the number of thermal neutrons in the region of measurement, compared with the case where the south face is a boundary to air. This point was tested experimentally, and it was found that the removal of the wax caused a maximum reduction in density of 10% in the first plane.

The experimental arrangement with the wax reflector was closer to the case of a square pile, bounded by air on all sides, than to the case of a semi-infinite pile in the z-direction, for calculation shows that the density of thermal neutrons at the first plane would be reduced by about 40% in going from the semi-infinite to the square pile. The effect of the wax was therefore to reduce

the ratio of fast to slow neutrons in the region of measurement up to 10%; and hence a slightly smaller correction for thermal sources is required than in the case of the finite pile.

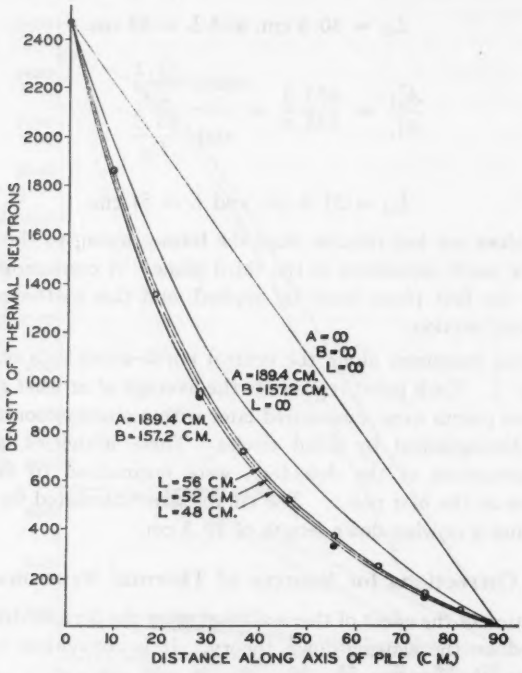

FIG. 3. *Measured densities of thermal neutrons along the central axis of the pile are shown by unfilled circles. Repetitions using a stronger source and after normalization with the previous measurements at the first plane are shown by filled circles. The lowest curves are those calculated for $L = 48$, 52, and 56 cm. and a slowing-down length of 20.8 cm. In addition, the curve is shown for $L = \infty$ (no capture), and the straight line for a pile infinite in the x- and y-directions and having $L = \infty$. Note that $A = a$ and $B = b$, the small letters being used in the text for two of the pile dimensions.*

(2) *Correction for Thermal Sources in the Case of the Finite Pile on the Basis of Elementary Slowing-down Theory*

The equation for χ, the number of neutrons per unit volume passing through the symbolic age $\theta = \int_0^t D\,dt$ in unit time, is

$$\frac{\partial \chi}{\partial \theta} = \nabla^2 \chi - \epsilon(\theta)\frac{\chi}{L^2} + S\,\delta\left(x - \frac{a}{2}\right)\delta\left(y - \frac{b}{2}\right)\delta(z - z_1)\,\delta(\theta + L_s^2) \quad (8)$$

(change of χ with age = influx − capture + source), where δ is Dirac's delta-operator, $\epsilon(\theta) = 0$ for $\theta < 0$ and $\epsilon(\theta) = 1$ for $\theta > 0$. $\theta = 0$ denotes the age at which neutrons become thermal and liable to be captured. L_s is the

slowing-down length to thermal velocities. S is the strength of the source (neutrons emitted per second) situated at $x = \frac{a}{2}$, $y = \frac{b}{2}$, $z = z_1$.

The boundary conditions for Equation (8) are $\chi = 0$ at $x = 0, a$; $\chi = 0$ at $y = 0, b$; and $\chi = 0$ at $z = 0, c$, where $c = 189.4$ cm. is the length of the pile in the z-direction.

We take, at first, the case of a pile infinite in the z-direction and later use images to fulfil the boundary conditions on z. The solution at $\theta = 0$ is

$$\chi(0) = \sum_{l,m} \frac{4}{ab} \frac{S}{\sqrt{4\pi L_s^2}} e^{\frac{-(z-z_1)^2}{4L_s^2}} e^{-\pi^2 L_s^2 \left(\frac{l^2}{a^2} + \frac{m^2}{b^2}\right)} \sin \frac{l\pi x}{a} \sin \frac{m\pi y}{b}$$

$$= \sum_{l,m} B_{lm}(x, y) \frac{e^{\frac{-(z-z_1)^2}{4L_s^2}}}{\sqrt{L_s^2}}$$

where $l, m = 1, 3, 5, \ldots\ldots$

This solution, representing the distribution of sources of thermal neutrons, is used as a boundary condition in solving Equation (8) for thermal neutrons ($\epsilon(\theta) = 1$). We obtain

$$\chi(\theta) = \sum_{l,m} \chi_{lm}(\theta) \quad \text{with } \chi_{lm}(\theta) = B_{lm} \frac{e^{\frac{-(z-z_1)^2}{4(L_s^2+\theta)} - \frac{\theta}{L_{lm}^2}}}{\sqrt{L_s^2 + \theta}}.$$

Since $\chi(\theta)\, dt$ is the number of neutrons per unit volume passing through an age θ in time dt, the number of neutrons per unit volume in an age interval dt is given by

$$\chi(\theta)\, dt = \chi(\theta) \frac{dt}{d\theta} d\theta = \frac{\chi(\theta)}{D} d\theta,$$

and the total density of thermal neutrons is given by $\rho = \int_0^\infty \frac{\chi(\theta)}{D} d\theta$, where D is the diffusion coefficient of *thermal* neutrons.

$$\rho = \frac{1}{D} \int_0^\infty \sum_{l,m} \chi_{lm}(\theta)\, d\theta = \sum_{l,m} \rho_{lm},$$

where

$$\rho_{lm} = \frac{1}{D} \int_0^\infty \chi_{lm}(\theta)\, d\theta.$$

$$\rho_{lm} = B_{lm} \frac{e^{L_s^2/L_{lm}^2}}{D} L_{lm} \sqrt{\frac{\pi}{2}} \left\{ e^{\frac{z_1 - z}{L_{lm}}} \left[1 - erf\left(\frac{L_s}{L_{lm}} + \frac{z_1 - z}{2L_s}\right)\right] + e^{\frac{-(z_1 - z)}{L_{lm}}} \left[1 - erf\left(\frac{L_s}{L_{lm}} - \frac{z_1 - z}{2L_s}\right)\right] \right\}.$$

An equivalent treatment has been given by Wallace and LeCaine (5).

The boundary conditions in the z-direction are now introduced by superposing the solutions for image sources about the two boundaries, viz., for

sources of alternate sign at distances $\pm (2nc - z_1)$, where n is an integer. For the region $15 < z < 89$ cm., between the first and third planes, we need only consider the primary source and three images. The first Fourier component of the density for the four sources is the only term for which the correction for thermal sources may be a significant fraction of the total density. Neglecting contributions of less than 0.1%, it reduces to the following:

$$\rho_{11} = C_{11}\left\{4\left(e^{\frac{-z_1}{L_{11}}} - e^{\frac{-(2c-z_1)}{L_{11}}}\right)\sinh\frac{z}{L_{11}} + e^{\frac{z_1-z}{L_{11}}}\left[1 - erf\left(\frac{L_s}{L_{11}} + \frac{z_1 - z}{2L_s}\right)\right] - e^{\frac{-(z_1+z)}{L_{11}}}\left[1 - erf\left(\frac{z_1 - z}{2L_s} - \frac{L_s}{L_{11}}\right)\right]\right\}, \qquad (9)$$

where

$$C_{11} = B_{11}\frac{e^{L_s^2/L_{11}^2}}{2D}L_{11}\sqrt{\pi}.$$

An estimate of the slowing-down length L_s may be made from measurements taken by Dr. L. G. Elliott. He used indium resonance detectors and the same source in this pile. It is sufficient for the present purpose to state that a single Gaussian curve fits the measured distribution near the source if the slowing-down length to indium resonance (1.44 ev. (2)) is taken between 16 and 17 cm. A single Gaussian curve fits the measured points farther from the source if the slowing-down length is taken to be 19 cm. Allowing for slowing-down from the indium resonance region to the region of capture by dysprosium, L_s was taken to be between 18 and 21 cm.

Equation (9) for ρ_{11} differs from Equation (5), where the variation of ρ_{11} with z is given by $\sinh\frac{z}{L_{11}}$, by the last two terms in the bracket. Using $L = 50$ cm., we find that these two terms amount to -2.2% for $L_s = 20.8$ cm., -1.5% for $L_s = 20$ cm., and -0.7% for $L_s = 18.5$ cm. at the first plane, and become negligibly small for distances from the source greater than 100 cm., i.e., in the region of the second plane.

The curves of Fig. 3 were computed using $L_s = 20.8$ cm. in Equation (9) for ρ_{11}, and the higher components from Equation (5).

(3) *Modification of the Slowing-down Theory*

In Part (2) the contribution of thermal sources to the density was calculated on the basis of elementary slowing-down theory. Using a better approximation of the transport theory, for which we are indebted to Dr. R. E. Marshak, it is found that the additional correction to the density up to distances of 100 cm. from the source never amounts to more than 25% of the correction found in Part (2).

The final correction to the density for thermal sources is approximately 1% at the first plane, and if A_{11} is increased by this amount, the value of L calculated from the ratio A_{11}/A'_{11} is reduced to 51 cm.

In Fig. 3 the calculated curves are normalized to the density at the first plane. The best value of L to fit the points on the central axis between 18 and 65 cm. from the first plane (i.e., in the region where the sensitivity of L is greatest) is 51 cm., with a probable error of about 3 cm.

For this graphite of average pile density 1.55 gm. per cc. the diffusion length is 51 $\pm$ 3 cm.

Limitation of Accuracy

The density measurements were limited in accuracy by the rather low counting rates, instability of the counter sensitivity, and the unsatisfactory reproducibility of geometry at the counter.

The size of the graphite pile was insufficient for good accuracy, which may be seen from Fig. 3. The straight line shown in this figure represents the variation of density along the axis of a pile infinite in the x- and y-directions (no leakage of neutrons through its sides) and $L = \infty$ (no capture). The next curve refers to the experimental pile as regards dimensions (same leakage) but having $L = \infty$ (no capture). It is clear that for a pile with this cross-section the leakage of neutrons is more important than the capture within the graphite. The same point may be shown algebraically. The relaxation length L_{11} of the first component in the harmonic analysis is given by

$$\frac{1}{L_{11}^2} = \frac{1}{L^2} + \pi^2\left(\frac{1}{a^2} + \frac{1}{b^2}\right) = 384 \times 10^{-6} + 675 \times 10^{-6}, \text{ or } L_{11} = 30.7 \text{ cm.}$$

The second or leakage term is 1.8 times the first or capture term.

Acknowledgments

We are grateful for permission to refer to unpublished work of the following: Dr. G. Placzek, Dr. W. Seidel, Dr. P. R. Wallace, Dr. Jeanne LeCaine, Dr. R. E. Marshak, and Dr. L. G. Elliott.

We have been greatly assisted by Miss E. O'Brien, who did part of the counting.

References

1. Hopf, L. Mathematical problems of radiative equilibrium. Cambridge tract No. 31 : 85. 1934.
2. Marshall, J. Bull. Am. Phys. Soc. 21 (3) : 12. 1946.
3. Placzek, G. and Seidel, W. Milne's problem in transport theory. Montreal report. 1943.
4. Smyth, H. D. Atomic energy for military purposes. Princeton Univ. Press. Princeton, N.J. 1945.
5. Wallace, P. R. and LeCaine, J. Elementary approximations in the theory of neutron diffusion. Montreal report. 1943.

THE DIFFUSION LENGTH OF THERMAL NEUTRONS IN HEAVY WATER CONTAINING LITHIUM CARBONATE[1]

By H. G. Hereward[2], G. C. Laurence[3], A. M. Munn[4], H. R. Paneth[2], and B. W. Sargent[3]

Abstract

The density distribution of thermal neutrons was measured with a small boron trifluoride chamber in a cylindrical tank containing 113 litres of heavy water in which lithium carbonate was dissolved. The diffusion length was found to be 22.7 cm. in this solution containing 7.70×10^{-4} atoms of lithium per molecule of heavy water (99.4 atom % D). After corrections were applied for the capture of neutrons in the heavy water and light hydrogen, the capture cross-section of lithium was found to be 59×10^{-24} cm.^{2} per atom for neutrons of standard velocity 2200 m. per sec. from the measured diffusion length and known transport mean free path.

Introduction

The diffusion length of thermal neutrons in a solution of a uranium compound in heavy water is not easy to measure directly owing to multiplication. If the ratio of the capture cross-section of uranium to that of boron or lithium is known, measurement of the diffusion length in a solution of a boron or lithium compound leads to the diffusion length in a uranium solution.

While the cross-section of boron is perhaps better known than that of lithium, there is a strong reason against its use and in favour of the use of lithium. Not only must the compound to be dissolved in heavy water be free of ordinary water and impurities that capture thermal neutrons strongly, but it must be possible to remove it completely from the heavy water by distillation. Mr. J. Hébert and Dr. A. G. Maddock (7) have kindly investigated these points for us, and found that the distillates from borax solutions contain boron, but that the lithium carbonate available in this laboratory meets all the requirements.

The density distribution of thermal neutrons was explored with a small boron trifluoride chamber in a cylindrical tank containing 113 litres of heavy water in which was dissolved sufficient lithium carbonate to reduce the diffusion length to a suitable value for measurement. In this solution containing 7.70×10^{-4} atoms of lithium per molecule of water (99.4 atom % D), the diffusion length was found to be 22.7 cm. This experiment was done in the Montreal Laboratory during the winter of 1944 and described in a report bearing the date May 16, 1944.

[1] *Manuscript received August 29, 1946.*

Contribution from the Physics Branch, Montreal Laboratory, Atomic Energy Division of the National Research Council of Canada. Publication has been delayed owing to security restrictions. Issued as N.R.C. No. 1470.

[2] *Member of United Kingdom Staff.*

[3] *Research Physicist, National Research Council, now at Chalk River, Ont.*

[4] *Junior Research Physicist, National Research Council, now at McGill University, Montreal, Que.*

Theory of the Experiment

The diffusion equation in the absence of thermal sources is

$$\nabla^2\rho - \frac{\rho}{L^2} = 0, \tag{1}$$

where ρ, the density of thermal neutrons, is a function of the co-ordinates, and L is the diffusion length (8). Equation (1) written in cylindrical co-ordinates r and z is

$$\frac{\partial^2\rho}{\partial r^2} + \frac{1}{r}\frac{\partial\rho}{\partial r} + \frac{\partial^2\rho}{\partial z^2} - \frac{\rho}{L^2} = 0\,. \tag{2}$$

The origin is taken at the centre of a horizontal cross-section near the bottom of the tank, and the positive direction of the z-axis is upwards along the axis of the tank. The term involving the angular co-ordinate θ is omitted from Equation (2). Any angular asymmetry found experimentally can be allowed for by taking the angular average of the measured density ρ for a given radial distance r and given height z.

The solution of Equation (2) is subject to four boundary conditions.

(1) The density ρ is finite on the axis of the cylinder.

(2) The density vanishes at the surface of a vertical coaxial cylinder of radius R, where R (evaluated later) is the effective radius of the tank;

$$\text{i.e. } \rho\,(r, z) = 0 \text{ for } r = R.$$

(3) The density vanishes at a horizontal plane a short distance above the surface of the liquid;

$$\text{i.e. } \rho\,(r, z) = 0 \text{ for } z = h \text{ (to be evaluated later).}$$

(4) The density distribution in the horizontal plane through the origin is given by measurement.

The desired solution of Equation (2) is

$$\rho = \sum_{n=1,2,3,\ldots} A_n J_0\,(\lambda_n r)\,\frac{\sinh\dfrac{h-z}{b_n}}{\sinh\dfrac{h}{b_n}}\,, \tag{3}$$

where

$$\frac{1}{b_n^2} = \lambda_n^2 + \frac{1}{L^2}\,. \tag{4}$$

The b_n's are the relaxation lengths of the various Fourier–Bessel components.

The λ_n's can be found from the roots of the equation: $J_0(\lambda_n R) = 0$;

$$\text{i.e. } \lambda_1 = \frac{2.4048}{R}\,, \quad \lambda_2 = \frac{5.5201}{R}\,, \quad \lambda_3 = \frac{8.6537}{R}\,,$$

$$\lambda_4 = \frac{11.792}{R}\,, \quad \lambda_5 = \frac{14.931}{R}\,, \text{ etc.}$$

Boundary condition (4) may be written

$$\rho(r, z = 0) = \sum_{n=1,2,3,\ldots} A_n J_0(\lambda_n r)\,. \tag{5}$$

This horizontal plane containing the origin must be taken a few scattering mean free paths above the bottom of the tank to avoid effects of scattering in the materials below the heavy water.

The density distribution was measured in three horizontal planes spaced at 12-cm. intervals, and along the central axis. The lowest or first plane was approximately 4.2 cm. above the bottom of the tank. The distributions were analysed transversely into Fourier–Bessel series, and the first component was thereby isolated. Its diminution in the vertical direction permitted b and h to be found according to Equation (3). The diffusion length was derived from Equation (4).

Experimental Details

The source of thermal neutrons was a graphite pile 186 cm. by 186 cm. in horizontal section and 274 cm. high. On the vertical axis of the pile and 100 cm. from the top was placed 2.2 gm. of radium mixed with beryllium. Since the distance from this source of fast neutrons to the cylindrical tank on top of the pile was five slowing-down lengths, neutrons entering the tank were almost entirely thermal ($> 99\%$ in number).

The graphite pile was covered on its sides, top, and bottom with cadmium sheet, 0.4 mm. thick. A wooden platform, 3.5 cm. thick, rested on the cadmium on top of the pile. Circular holes, 65 cm. in diameter, in the cadmium top and in the platform, were centred roughly on the axis of the pile. A circular aluminium tray, 91 cm. in diameter, was placed symmetrically over these holes to catch any leakage of heavy water in case of accidents, after the space between the graphite blocks and the upper surface of the wooden platform had been packed with petroleum coke and levelled. The experimental tank (Fig. 1) was centred in the tray. This tank was made of aluminium of wall thickness 3.3 mm. and 45.4 cm. high. Its internal diameter was measured in several directions and at various heights with a suitable inside caliper made for the purpose. The individual measurements were between 61.16 and 60.94 cm., and the average diameter was 61.01 cm.

The cover of the tank was designed with the assistance of Dr. S. G. Bauer. A glass disk, 7 mm. thick and 69.7 cm. in diameter, rested on the upper flange of the tank, and the joint was sealed with Apiezon grease *M*. A radial slot, 35 cm. long and 2.6 cm. wide, along which the boron chamber could be moved, was cut in the disk. A glass slab, 42 by 10 cm., with an identical slot, was cemented on to the disk so that the two slots coincided. A second slab, 76 by 13 cm., with a conical hole for the gland supporting the boron chamber, rested on the upper greased surface of the first slab. A tall box housing the head amplifier and gland for the boron chamber was clamped on the movable slab. The sides of the tank were tightly wrapped with cadmium sheets, and similar sheets were placed on top of the glass disk and slabs.

A number of excellent boron chambers were made for us by Mr. N. A. Veall (11); one of these is shown in Fig. 2. The chambers were made of lead glass, 5 mm. in internal diameter and 0.45 cc. in volume, and were filled with boron

trifluoride to a pressure of about 2 atm. The guard-rings were grounded in the solution. The first chamber was sealed to the lower end of a single glass tube housing the lead to the central anode. The high tension lead to the platinum cathode was a rubber-insulated wire to the lower end of the chamber and the joint was made water-tight with rubber Bostik. After some time the

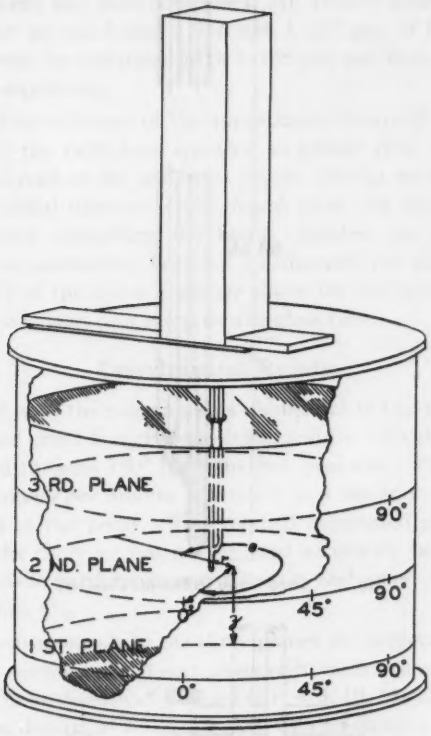

FIG. 1. *Experimental tank. The boron chamber and head amplifier box are shown.*

insulation failed, and this chamber was replaced by a second chamber sealed to two parallel glass tubes, one tube housing the lead to the anode, and the other the high tension wire to the cathode (Fig. 2). The latter tube was filled with some of the solution to reduce the disturbance in the neutron distribution caused by the channel. The glass tubes to the chamber were clamped in a gland, and the height was adjustable. The gland for the second boron chamber, designed by Mr. N. Q. Lawrence and Mr. N. A. Veall, is shown in Fig. 3.

The counting equipment was supplied by Mr. H. F. Freundlich. It consisted of a head amplifier (5), mounted as closely as possible to the boron

chamber, a linear amplifier of four stages, a discriminator to reject pulses below a chosen size, a scale-of-32, and an oscilloscope. A stabilized high

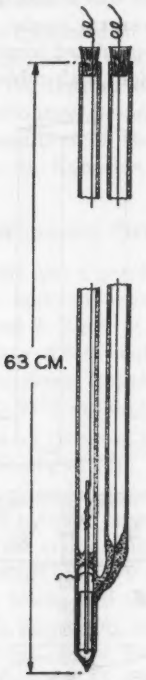

FIG. 2. *Small boron trifluoride chamber.*

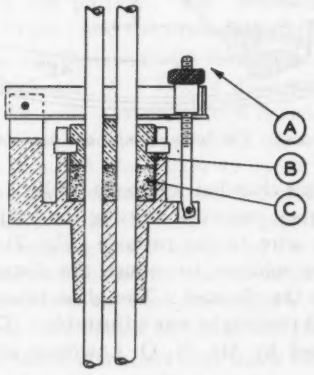

FIG. 3. *Gland to support boron chamber. Tightening the nut A pushes the brass piece B on to the graphitized rubber gasket C, thus making a tight joint.*

voltage (usually about 800 v.) was applied to the boron chambers. All electrical leads were shielded, and all units were brought to a common ground.

The solution of lithium carbonate was made by stirring 179.73 gm. of the carbonate in 125.2 ± 0.1 kgm. of heavy water for a period of three hours. A portion (125.1 kgm.) of the solution was placed in the experimental tank. After the experiment had been completed, Mr. Hébert analysed two samples of the solution for us and found 1.566 and 1.575 gm. of lithium carbonate per litre, which may be compared with 1.585 gm. per litre from the original weights of the components.

The cylindrical co-ordinates of the approximate centre of sensitivity of the boron chamber in the tank were specified as follows (Fig. 1). The angular co-ordinate θ was read at the axial slot on the circular scale painted around the tank. The radial distance r was found from the displacement of the movable glass plate supporting the boron chamber, the glass disk being centred through measurements between its edge and the upper flange of the tank. The height of the boron chamber above the first plane was measured from a mark on the gland to a mark on the glass tube.

Experimental Results

At any point (r, z, θ) the counting was carried out in two parts, (i) with the boron chamber and gland in a given position, and (ii) with the boron chamber and gland rotated through 180° from the first position. The average of the two readings in counts per minute was taken as a measure of the density of thermal neutrons at the point. This method eliminated possible error due to the fact that the chamber was not situated accurately below the centre of the gland. Sufficient particles were counted at each point for the statistical error to be less than 1%.

Most of our measurements in the three planes are summarized in Table I. In the first plane, readings were taken along eight radii spaced at 45° intervals. That is, for $z = 0$, the densities at values of $r = 5, 10, 15, 17.5$ cm., etc. were compared with the density at $r = 0$ for eight different angles θ. The readings were normalized to a count at the centre of 700 particles per minute, which was approximately the observed counting rate. Similar measurements were made in the second plane, which was 12 cm. above the first plane. In this case readings were normalized to a count at the centre of 270 particles per minute (see Table II). A slight angular asymmetry appeared in both planes, and it was traced to variations in depth due to the fact that the bottom of the tank was not perfectly flat and also to a slight error in levelling. The asymmetry was removed by averaging the densities for a given r and z over the angle θ. In the third plane, 12 cm. above the second, it was sufficient to measure along four radii. These readings were normalized to a count at the centre of 91 particles per minute (see Table II). The average densities are plotted against the radial distances in Fig. 4.

TABLE I

EXPERIMENTAL RESULTS

DENSITY ρ AT VARIOUS ANGLES θ

r, cm.	0°	45°	90°	135°	180°	225°	270°	315°	*Av.
First plane									
0	700	700	700	700	700	700	700	700	700
5	690	682	—	683	691	—	—	—	686
10	637	637	640	649	652	636	641	641	642
15	567	568	568	585	578	571	574	560	571
17.5	520	516	535	532	532	530	517	520	525
20	457	458	470	481	472	460	460	463	465
22.5	392	393	409	415	406	405	390	394	401
25	314	320	331	330	328	322	307	308	320
27.5	—	—	—	—	—	—	218	—	222
Second plane									
0	270	270	270	270	270	270	270	270	270
5	—	263	—	263	261	—	—	258	261
10	235	240	241	238	244	242	236	235	239
15	197	208	210	207	207	206	202	207	205
17.5	184	181	—	181	181	—	181	178	181
20	153	153	160	161	160	158	157	151	157
22.5	124	125	129	126	128	—	125	—	126
25	92.7	96.4	97.0	99.0	96.5	100	94.8	92.0	96.0
27.5	—	—	—	—	—	—	62.0	—	62.5
Third plane									
r, cm.	0°		90°		180°		270°		*Av.
0	91		91		91		91		91
5	85.5		89.5		87.5		86.7		87.3
10	80.5		78.1		79.0		79.6		79.3
15	67.0		68.6		65.9		65.4		66.7
17.5	—		59.5		58.5		60.5		59.5
20	48.5		50.6		49.0		49.4		49.4
22.5	—		39.5		—		39.8		39.6
25	—		30.3		29.4		29.8		29.8
27.5	—		—		—		18.0		18.0

** In the last line ($r = 27.5$ cm.), where there is a single measurement at $\theta = 270°$, the average over all angular positions takes into account the angular asymmetry in this position judged from the measurements at neighbouring points and the contour map of the bottom of the tank.*

The density distribution along the central axis was also measured with the two boron chambers, and the averages at points spaced at 2-cm. intervals are plotted in Fig. 5. The densities at the centres of the second and third planes were each compared many times with the density at the centre of the first plane. These results including the averages of the residuals are given in Column 2 of Table II.

TABLE II

COMPARISON OF THE DENSITIES OF THERMAL NEUTRONS AT THE CENTRES OF THREE PLANES

Plane No.	Boron chamber at end of vertical tubes		Boron chamber at end of L-shaped tubes	
	Density	No. of comparisons	Density	No. of comparisons
1	700	—	700	—
2	270 ± 3	11	271 ± 4	11
3	91.0 ± 1.9	12	89.3 ± 2.3	8

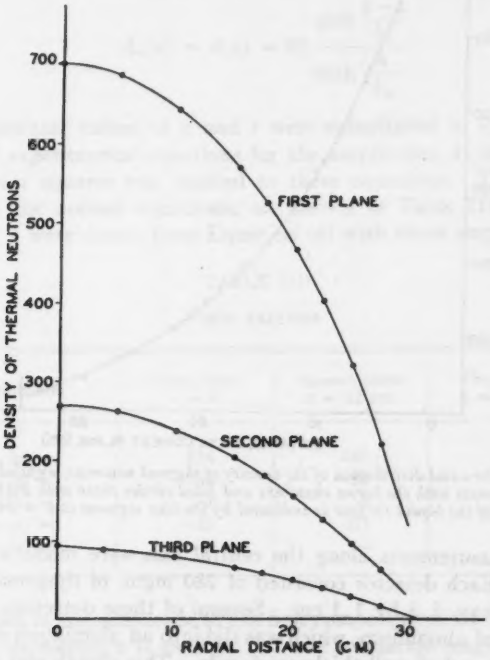

FIG. 4. *The radial distribution of the density of thermal neutrons.*

All measurements taken with the two different boron chambers agreed closely and were independent of the bias-setting of the discriminator and of the potential difference across the boron chambers. In order to ascertain whether there was any disturbance in the neutron density caused by the hollow glass tube supporting the boron chamber, the tubes of the second boron chamber were bent into an L-shape so that the centre of sensitivity of the chamber was displaced 10.2 cm. horizontally from the vertical supporting

tubes, and the intensities at the centres of the three planes were again compared. From a comparison of these results in Column 4 with those in Column 2 of Table II it is clear that the channel effect is small.

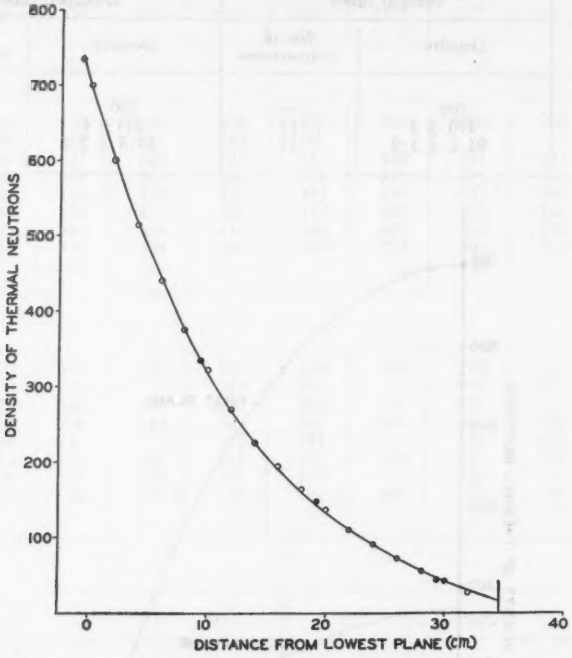

FIG. 5. *The axial distribution of the density of thermal neutrons, unfilled circles representing measurements with the boron chambers and filled circles those with dysprosium detectors. The position of the liquid surface is indicated by the line segment at* $z = 34.6$ *cm.*

A few measurements along the central axis were made with dysprosium detectors. Each detector consisted of 280 mgm. of dysprosium oxide in an aluminium tray, 2.3 by 1.1 cm. Several of these detectors were spaced on a thin strip of aluminium, which was slid into an aluminium sheath of oblong cross-section and of wall thickness 5 mils. This sheath was supported at its top by a cone that fitted into the hole in the movable glass slab. Our counting procedure for activated detectors has been described in a previous paper (8). The measurements with the dysprosium detectors are fitted to the measurements with the boron chambers in Fig. 5, where the agreement is seen to be satisfactory.

Analysis of the Experimental Results

Before the transverse measurements could be analysed into Fourier–Bessel series the parameters λ_n had to be estimated. This step required the value of the effective radius R. In our first analysis, R was taken to be equal to

the internal radius of the tank, plus 0.05 cm. for the aluminium wall of actual thickness 0.33 cm., plus 1.65 cm. This last length was the intercept of the curve, showing the density of thermal neutrons in a sample of the same heavy water as a function of the distance from a flat cadmium boundary, obtained in an experiment by Auger, Munn, and Pontecorvo (1).

$$R = 30.50 + 0.05 + 1.65 = 32.2 \text{ cm.}$$

$\lambda_1 = 0.074684$, $\lambda_2 = 0.17143$, $\lambda_3 = 0.26875$, $\lambda_4 = 0.36620$, $\lambda_5 = 0.46369$ cm.$^{-1}$

The density distribution in each plane may be written

$$\rho = \sum_{n=1,2,3,\ldots} A_n(z) J_0(\lambda_n r), \tag{6}$$

where

$$A_n(z) = A_n(z=0) \frac{\sinh \frac{h-z}{b_n}}{\sinh \frac{h}{b_n}}.$$

The experimental values of ρ and r were substituted in Equation (6) to form a set of experimental equations for the amplitudes $A_n(z)$. Legendre's method of least squares was applied to these equations. The amplitudes, derived from the normal equations, are shown in Table III. The curves shown in Fig. 4 were drawn from Equation (6) with these amplitudes.

TABLE III

FIRST ANALYSIS

Amplitude	First plane $z = 0$	Second plane $z = 12$ cm.	Third plane $z = 24$ cm.
$A_1(z) =$	814	287	94
$A_2(z) =$	−156	−22	−3
$A_3(z) =$	57	4	—
$A_4(z) =$	−23	(1)	—
$A_5(z) =$	8	—	—

The reduction in the amplitude of the first component of the Fourier–Bessel analysis with increasing z is used to find the relaxation length. When the three planes are equally spaced, two useful formulae can be derived from Equation (3). Let $A_1(z_1)$, $A_1(z_1 + c)$, and $A_1(z_1 + 2c)$ be the amplitudes of the first component in the planes having vertical co-ordinates z_1, $z_1 + c$, and $z_1 + 2c$, respectively. It is easy to show that

$$\cosh \frac{c}{b_1} = \frac{1}{2} \frac{A_1(z_1) + A_1(z_1 + 2c)}{A_1(z_1 + c)} \tag{7}$$

$$\text{and } \tanh \frac{h - z_1 - c}{b_1} = \frac{A_1(z_1) + A_1(z_1 + 2c)}{A_1(z_1) - A_1(z_1 + 2c)} \tanh \frac{c}{b_1}. \tag{8}$$

Similar expressions may be written for other components. From Equations (7) and (8) and the amplitudes (before rounding off their values for Table III)

$$b_1 = 11.63 \text{ cm.}$$
$$h = 37.6 \text{ cm.}$$

From Equation (4) $L = 23.5$ cm.

If the corresponding equations are applied to the second and third components, we find that L is imaginary. Two possible explanations for this behaviour may be suggested. (i) Since the relaxation length for the second component is only 5.7 cm., as compared with 2.3 cm. for the transport mean free path, the diffusion theory may be greatly in error for components higher than the first. (ii) Since $1/L^2$ is only 6% of λ_2^2 (but 33% of λ_1^2), the determination of L from the second (and higher components) is too dependent on λ and hence on the effective radius. As there is some doubt regarding the contribution of the aluminium wall of the tank to the effective radius, a value of 32.5 cm. for the radius is admissible. Using $R = 32.5$ cm. and

$$\lambda_1 = 0.073995, \lambda_2 = 0.16985, \lambda_3 = 0.26627, \lambda_4 = 0.36282, \lambda_5 = 0.45941 \text{ cm.}^{-1}$$

the amplitudes $A_n(z)$ of Table IV were obtained by the method of least squares. From Equations (7), (8), and (4)

TABLE IV

SECOND ANALYSIS

Amplitude	First plane $z = 0$	Second plane $z = 12$ cm.	Third plane $z = 24$ cm.
$A_1(z) =$	808	285	93
$A_2(z) =$	−144	−18	−2
$A_3(z) =$	47	2	—
$A_4(z) =$	−15	—	—
$A_5(z) =$	4	—	—

and the amplitudes (before rounding off their values for Table IV)

$$b_1 = 11.62 \text{ cm.}$$
$$h = 37.7 \text{ cm.}$$
$$L = 22.7 \text{ cm.}$$
$$b_2 = 5.78 \text{ cm.}$$
$$L = 30 \text{ cm.}$$

It would be possible to derive a perfectly consistent set of values of L from the first and second components by choosing a suitable value of R very close to 32.5 cm.

A comparison of the analyses for radii of 32.2 and 32.5 cm. with the experimental results in Table V shows that it is impossible to choose between them on the basis of best fit. However, a change of 1% in the effective radius

TABLE V

COMPARISON OF EXPERIMENTAL RESULTS AND ANALYSES

r, cm.	ρ, exp.	ρ, calc.	
		R = 32.2 cm.	R = 32.5 cm.
First plane			
0	700	700	700
5	686	684	685
10	642	643	643
15	571	571	571
17.5	525	523	523
20	465	466	467
22.5	401	401	400
25	320	321	319
27.5	222	222	222
Second plane			
0	270	270	269
5	261	262	262
10	239	239	240
15	205	204	204
17.5	181	182	181
20	157	156	155
22.5	126	127	127
25	96.0	95.4	95.8
27.5	62.5	62.1	63.7
Third plane			
0	91.0	91.0	91.0
5	87.3	88.3	88.2
10	79.3	80.2	79.9
15	66.7	67.0	66.6
17.5	59.5	58.7	58.4
20	49.4	49.6	49.4
22.5	39.6	39.7	39.7
25	29.8	29.4	29.6
27.5	18.0	18.9	19.5

causes only a 4% change in L derived from the first component. We have no information on the breakdown of diffusion theory for components higher than the first, which was mentioned as a possible explanation of the internal inconsistency found in the first analysis. Accordingly, we slightly prefer the second analysis with its better internal consistency, and shall write for the final result:

$$L = 22.7 \text{ cm.}$$

The axial measurements support, but do not throw new light on, the value of the diffusion length just derived. In Fig. 5 the measurements taken at

2-cm. intervals are shown to be in good agreement with the curve plotted from Equation (3) with the following constants:

$$R = 32.5 \text{ cm.}, L = 22.7 \text{ cm.}, h = 37.7 \text{ cm.},$$

$$A_1 = 808, A_2 = -144, A_3 = 47, A_4 = -15 \text{ and } A_5 = 4.$$

While the liquid surface is shown in Fig. 5 at 34.6 cm. above the first plane, this value can be only approximate, as the centre of sensitivity of the boron chamber was not accurately located. (The chamber counts over a length between 2.0 and 2.6 cm.) Owing to this reason and to the scattering of neutrons from the glass cover it is not possible to evaluate h from the position of the liquid surface and the value of the cut-off distance in the absence of back-scattering. From an inspection of Fig. 5, h must lie between 36.0 and 38.5 cm. However, the diffusion length is determined mainly from the measurements deep within the solution and is therefore not very much dependent on h.

The effect of errors in the observations on the derived diffusion length can be seen from the following considerations. The density distribution of thermal neutrons obeys the differential Equation (2), which may be written:

$$\frac{1}{L^2} = \frac{\frac{\partial^2\rho}{\partial r^2} + \frac{1}{r}\frac{\partial\rho}{\partial r}}{\rho} + \frac{\frac{\partial^2\rho}{\partial z^2}}{\rho}. \tag{9}$$

With reference to Fig. 4, it is found by trial that if the curve is altered by changing $\left(\frac{\partial^2\rho}{\partial r^2} + \frac{1}{r}\frac{\partial\rho}{\partial r}\right) / \rho$ by 3% throughout its length, it no longer fits the experimental points well. Similarly, a change of 3% in $\frac{\partial^2\rho}{\partial z^2} / \rho$ in the curve of Fig. 5 gives a poor fit with the points. The two right-hand terms in Equation (9) are roughly in the ratio $-3 : 4$ or better, except near the wall of the tank where less weight is attached to the observations. From the separate estimates the resulting error in L cannot exceed

$$\frac{1}{2}\left\{\left|\frac{-3}{4-3}\right| 3\% + \left|\frac{4}{4-3}\right| 3\%\right\} = 10\%.$$

Other errors, such as that in the concentration of lithium, and those due to the channel effect and shift of the centre of sensitivity of the boron chamber as it is raised in the solution, are comparatively negligible (Table II). By calculation it is found that the shift of the centre of sensitivity of the chamber causes a change in the counting rate of less than 0.1%, which is beyond detection.

Discussion

On the basis of diffusion theory it is possible to calculate any one of the three quantities — diffusion length L, transport mean free path l_t, and capture mean free path l_c — provided that the others are given, for

$$L^2 = \frac{1}{3} l_t l_c. \tag{10}$$

Auger, Munn, and Pontecorvo (1) have found l_t to be 2.31 cm. in a sample of the same heavy water as used here for the measurement of the diffusion length. Since the amount of lithium carbonate dissolved in the water is too small to affect its scattering properties, $l_t = 2.31$ cm. in the solution. Substituting $L = 22.7$ cm. and $l_t = 2.31$ cm. in Equation (10),

$$l_c = 669 \text{ cm.}$$

$$\text{and } \Sigma n\sigma = \frac{1}{l_c} = 149 \times 10^{-5} \text{ cm.}^{-1}$$

n is the number of atoms (or molecules) per cubic centimetre of the constituent, and σ is the capture cross-section per atom (or per molecule), the sum being taken for the constituents D_2O, H_2O, and Li_2CO_3 in the solution. In order to derive the capture cross-section of lithium, we shall allow for the capture of neutrons by the heavy and light water,* and neglect the capture by the carbon and oxygen of the carbonate and the oxygen of the light water present.

For D_2O $\quad n = 3.33 \times 10^{22}$ molecules per cc.

For H_2O $\quad n = \frac{0.60}{100} \times 3.33 \times 10^{22} = 2.0 \times 10^{20}$ molecules per cc.,

based on mass spectroscopic analyses carried out in Dr. H. G. Thode's laboratory. For lithium carbonate, 1.57 gm. per litre of solution,

$$n = 2.58 \times 10^{19} \text{ atoms lithium per cc.}$$

According to an argument to be given later, the capture cross-sections to be used here should be those for neutrons of velocity† 2500 m. per sec. Booker, Cavanagh, Hereward, Niemi, and Sargent (2) have found from a measurement of the diffusion length in heavy water that the capture cross-section is 0.81×10^{-27} cm.^{2} per molecule D_2O for neutrons of velocity 2500 m. per sec.

The capture cross-section of hydrogen will be found from the absolute cross-section of boron and the ratio of the cross-sections of boron and hydrogen. Dr. Fermi (4) informed us that the capture cross-section of boron is 705×10^{-24} cm^2. per atom for neutrons of velocity 2200 m. per sec. (Recently Marshall (9) has published his value of 710×10^{-24} cm.^{2} per atom, measured some time ago at the Argonne Laboratory.) The best measurement of σ_B / σ_H known to us is 2270, obtained by Whitehouse and Graham (12) of the Montreal Laboratory. From these results $\sigma = 0.548 \times 10^{-24}$ cm.^{2} per molecule H_2O for neutrons of velocity 2500 m. per sec.

For D_2O and H_2O together $\Sigma n\sigma = 14 \times 10^{-5}$ cm.$^{-1}$, which leaves 135×10^{-5} cm.$^{-1}$ for the $n\sigma$ of lithium.

The capture cross-section of lithium follows:

$$\sigma = 52 \times 10^{-24} \text{ cm.}^2 \text{ per atom.}$$

**For cross-section calculations it is immaterial whether we consider 1.2% HDO or its equivalent 0.6% H_2O.*

†We do not make the classic distinction between velocity and speed.

It will be seen from the considerations that follow that the cross-section found from the diffusion length and transport mean free path corresponds approximately to the average velocity of the neutron spectrum, which is about 2500 m. per sec. at room temperature. We assume that the transport mean free path in heavy water is independent of the neutron velocity, and therefore the diffusion coefficient

$$D = \frac{1}{3} l_t \bar{v},$$

where $\bar{v}$ is the average speed of the Maxwellian distribution of neutrons at room temperature. The diffusion length L may be written in terms of the diffusion coefficient D and the mean lifetime

$$\tau = \frac{1}{\Sigma n \sigma v}.$$

Since the capture cross-section of lithium varies inversely as the velocity, according to the measurements of Havens and Rainwater (6, 10), τ is independent of the velocity. Therefore

$$L^2 = D\tau = \frac{1}{3} l_t \bar{v} \tau = \frac{1}{3} l_t l_c,$$

where $l_c = \bar{v} \tau$ is the capture mean free path for the average velocity of the neutron spectrum, and hence σ found above is the capture cross-section corresponding to that velocity. Referring to a standard velocity of 2200 m. per sec., we have

$$\sigma \text{ (lithium)} = 59 \times 10^{-24} \text{ cm.}^2 \text{ per atom.}$$

In view of the assumptions and probable errors in the combined physical data just used, we conclude that this value is in agreement with 65×10^{-24} cm.^{2} communicated to us by Dr. Fermi (4) and 67×10^{-24} cm.^{2} obtained by Fenning, Graham, and Seligman (3) from their measured ratio σ_B / σ_{Li} and the Argonne Laboratory value $\sigma_B = 705 \times 10^{-24}$ cm.^{2} On the other hand, Havens and Rainwater (6, 10) have found higher values: $\sigma_B = 740 \times 10^{-24}$ cm.^{2} and $\sigma_{Li} = 72 \times 10^{-24}$ cm.^{2} for neutrons of velocity 2200 m. per sec.

Acknowledgments

We wish to thank our colleagues named in this paper for assistance in the design and construction of parts of the apparatus and in chemical and mass spectroscopic analyses. We are also grateful to several of our colleagues for permission to use unpublished information, and to Dr. E. Fermi for information privately communicated.

References

1. Auger, P., Munn, A. M., and Pontecorvo, B. The transport mean free path of thermal neutrons in heavy water. Montreal report. 1944.
2. Booker, D. V., Cavanagh, P. E., Hereward, H. G., Niemi, N. J., and Sargent, B. W. The diffusion length of thermal neutrons in heavy water. Montreal report. 1946.
3. Fenning, F. W., Graham, G. A. R., and Seligman, H. Ratio of the capture cross-sections of boron and lithium. Montreal report. 1944.

4. FERMI, E. Private communications from Argonne Laboratory. 1944.
5. FREUNDLICH, H. F. and LAWRENCE, N. Q. Report on design and construction of head amplifiers used at the Montreal Laboratory. 1944.
6. HAVENS, W. W., JR. and RAINWATER, J. Bull. Am. Phys. Soc. 21 (3) : 13. 1946.
7. HÉBERT, J. and MADDOCK, A. G. Relative merits of boron and lithium compounds as contaminating agents. Montreal report. 1944.
8. HEREWARD, H. G., LAURENCE, G. C., PANETH, H. R., and SARGENT, B. W. Can. J. Research, A, 25 : 15-25. 1947.
9. MARSHALL, J. Bull. Am. Phys. Soc. 21 (3) : 12. 1946.
10. RAINWATER, J. and HAVENS, W. W., JR. Bull. Am. Phys. Soc. 21 (3) : 13. 1946.
11. VEALL, N. A. On the construction of small boron chambers. Montreal report. 1944.
12. WHITEHOUSE, W. J. and GRAHAM, G. A. R. Ratio of the neutron absorption cross-sections of boron and hydrogen. Montreal report. 1945.

THE CALCULATION OF LINE STRENGTHS FROM LABORATORY DATA[1]

By William Petrie[2]

Abstract

A. S. King has made extensive intensity estimates of spectral lines in furnace and arc spectra, and these data provide useful material for determining line strengths. The estimates have been made for many elements of astrophysical interest, and are reduced to line strengths for FeI, TiI, and TiII.

Introduction

It is well to distinguish between two quantities, the strength, and the intensity, of a spectral line. The strength of a line is defined as the sum of the absolute squares of the matrix elements of electric moment joining the sets of states in question. On the other hand, the intensity of a line is proportional to the number of atoms in any one of the states of its initial level, the fourth power of its frequency, and its strength.

The line strength of the transition from an initial to a final level defined by the quantum numbers γLSJ and $\gamma' L'SJ'$, respectively, is

$$[(a \mid P \mid b)]^2 = \sum_{MM'} [(\gamma LSJM \mid P \mid \gamma' L'SJ'M')]^2, \tag{1}$$

where L = the orbital quantum number,
S = the spin quantum number,
J = the inner quantum number,
M = the magnetic quantum number,
γ = the sum of quantities other than $LSJM$ necessary to define a state.

Expression (1) enables one to calculate the relative strengths of the lines within a multiplet when LS coupling holds. Such line strengths have been calculated by White (8) and Russell (6).

Line strengths have also been obtained from solar data. The method has been fully described by Menzel (5) and more recently by Wright (9). The method is to obtain the so-called 'curve of growth' for a number of lines of the solar Fraunhofer spectrum, by plotting the theoretical strength of each line against the corresponding measured equivalent width. The equivalent width is a measure of the energy removed from the continuous spectrum by the absorption line. From the 'curve of growth,' the strength of any line may be obtained from the measured equivalent width. Solar line strengths are more numerous than the theoretical values, since all lines that have measurable equivalent widths are used. The solar line strengths also include intercombination lines, and these are absent from the theoretical values.

[1] *Manuscript received May 14, 1946.*
Contribution from the Department of Physics, University of Saskatchewan, Saskatoon, Sask.

[2] *Associate Professor.*

Beginning in 1913, and continuing the work over a long period of years, A. S. King has estimated the intensities of thousands of lines in the electric furnace and arc spectra. A description of the apparatus used and the procedure followed (1) in estimating intensities has been given. The eye estimates were made on a remarkably consistent scale, and self-reversal effects were indicated and allowed for when present. These data are useful for obtaining line strengths. It was pointed out by Russell (7) in 1925 that the square of King's estimated intensities are very nearly proportional to theoretical line strengths. This relation makes it possible to interpret King's estimated intensities in terms of line strengths. It will be indicated later that emission line theory yields the same results.

Calibration of the King Intensity Scale

The elements chosen for the initial work are FeI, TiI, and TiII. The lines are first divided into groups of the same excitation potential. For the lines of each group, a logarithmic plot is made between the squares of King's arc intensities as abscissae and the solar line strengths as ordinates. The solar line strength is called X'_0. Each resulting line segment now differs by the Boltzmann factor, $\frac{5040\ \Delta\chi}{T}$, which we call B. $\Delta\chi$ = the difference in excitation potential in electron volts of the lines in each group; T = the excitation temperature in degrees absolute of the arc. The excitation temperature of the arc is determined from the shift required to superimpose each line segment on the segment for the spectral lines of lowest excitation potential. If the shift is called Δy, then

$$\Delta y = \frac{5040\ \Delta\chi}{T}. \qquad (2)$$

This relation makes it possible to determine the excitation temperature of the arc.

Fig. 1 shows the resulting curves for FeI after superimposing the line segments. The points that are far off the line are probably affected by blending, and the general scatter is partly the result of departures from LS coupling. The wave-length range for each plot was chosen after studying the sensitivity curve of the photographic plates used by King. The range in sensitivity of the plates used for the wave-length regions chosen is small. Trial and error methods also show that the best curves are obtained when the data are divided in this manner.

Fig. 2 shows the temperature of the arc in degrees absolute as obtained from the data in the chosen wave-length regions. The temperature is seen to be a function of the excitation potential of the upper level involved in the production of each group of lines considered, which means that the arc is not in thermodynamic equilibrium. The excitation potential of the upper level is denoted by EP_H.

When the temperature of the arc is known from Fig. 2 we obtain values of line strengths from Fig. 1. For a given line we read off the value corresponding to the square of the logarithm of King's intensity, and then add the Boltzmann factor obtained from the temperature of the arc and the excitation

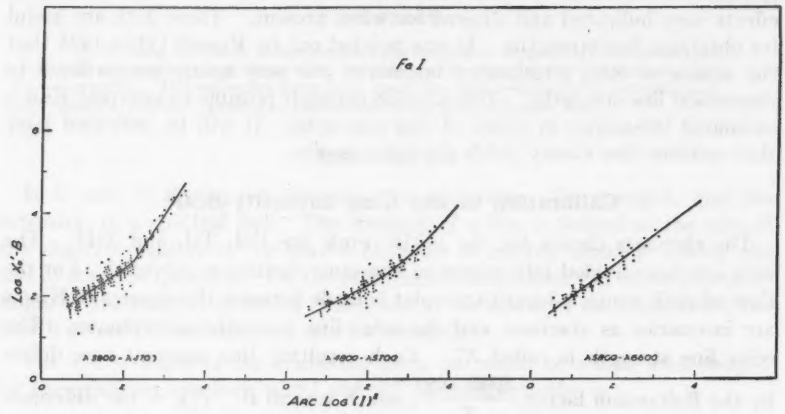

FIG. 1. *Calibration of the King intensity estimates.*

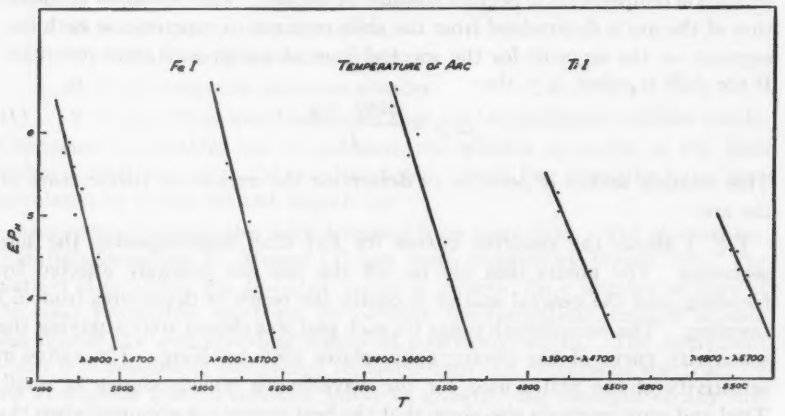

FIG. 2. *Excitation temperature of the arc.*

potential of the upper level involved in the production of the line. This calibration is extremely useful, since we can now obtain strengths for many hundreds of lines of FeI in the wave-length range λ 3900–λ 6600. In order to facilitate more rapid use of the calibration, a double entry table is constructed. Tables I(*a*), I(*b*), and I(*c*) give the value of the line strength desig-

nated as X'_0, corresponding to a given arc intensity and a given excitation potential. Tables II(a), II(b), II(c), and III give the same quantity for TiI and TiII.

TABLE I (a)

FeI—Log X'_0 values

King (I) arc \ EP_H	3.0	3.4	3.8	4.2	4.6	5.0	5.4	5.8	6.2	6.6	7.0
2	1.89	2.25	2.63	3.04	3.44	3.87	4.32	4.78	5.26	5.80	6.26
4	2.26	2.62	3.00	3.41	3.81	4.24	4.69	5.15	5.63	6.17	6.66
6	2.47	2.83	3.21	3.62	4.02	4.45	4.90	5.36	5.84	6.38	6.87
8	2.62	2.98	3.36	3.77	4.17	4.60	5.05	5.51	5.99	6.53	7.02
10	2.74	3.10	3.48	3.89	4.29	4.72	5.17	5.63	6.11	6.65	7.14
12	2.91	3.27	3.65	4.06	4.46	4.89	5.34	5.80	6.28	6.82	7.31
20	3.54	3.90	4.28	4.69	5.09	5.52	5.97	6.43	6.91	7.45	7.94
30	4.09	4.45	4.83	5.24	5.64	6.07	6.52	6.98	7.46	8.00	8.49
40	4.43	4.79	5.17	5.57	5.98	6.41	6.86	7.32	7.80	8.34	8.83
50	4.71	5.07	5.45	5.86	6.26	6.69	7.14	7.60	8.08	8.62	9.11

λ 3900 – λ4700

TABLE I (b)

FeI—Log X'_0 values

King (I) arc \ EP_H	3.0	3.4	3.8	4.2	4.6	5.0	5.4	5.8	6.2	6.6	7.0
2	2.08	2.46	2.85	3.26	3.68	4.12	4.57	5.05	5.52	6.02	6.56
4	2.39	2.77	3.16	3.57	3.99	4.43	4.88	5.36	5.83	6.33	6.87
6	2.57	2.95	3.34	3.75	4.17	4.61	5.06	5.54	6.01	6.51	7.05
8	2.70	3.08	3.47	3.88	4.30	4.74	5.19	5.67	6.14	6.64	7.18
10	2.82	3.20	3.59	4.00	4.42	4.86	5.31	5.79	6.26	6.76	7.30
12	2.93	3.31	3.70	4.11	4.53	4.97	5.42	5.90	6.37	6.87	7.41
15	3.08	3.46	3.85	4.26	4.68	5.12	5.57	6.05	6.52	7.02	7.56
20	3.25	3.63	4.02	4.43	4.85	5.29	5.74	6.22	6.69	7.19	7.73
25	3.40	3.78	4.17	4.58	5.00	5.44	5.89	6.37	6.84	7.34	7.88
30	3.52	3.90	4.29	4.70	5.12	5.56	6.01	6.49	6.96	7.46	8.00
35	3.64	4.02	4.41	4.82	5.24	5.68	6.13	6.61	7.08	7.58	8.12
40	3.74	4.12	4.51	4.92	5.34	5.78	6.23	6.71	7.18	7.68	8.22
50	3.92	4.30	4.69	5.10	5.52	5.96	6.41	6.89	7.36	7.86	8.40
60	4.07	4.45	4.84	5.25	5.67	6.11	6.56	7.04	7.51	8.01	8.55
75	4.27	4.65	5.04	5.45	5.87	6.31	6.76	7.24	7.71	8.21	8.75
100	4.52	4.90	5.29	5.70	6.12	6.56	7.01	7.49	7.96	8.46	9.00

λ 4800 – λ5700

The question arises whether or not the approximation $(I)^2$ proportional to line strength is sufficiently accurate. The emission in a spectral line in ergs per second from an emitting volume of 1 cm.^{3} is given by the following relation:

$$I = \frac{64\,\pi^4\nu^4}{3c^3}\,\frac{N_0}{\tilde{\omega}_0}\,e^{-\chi_s/kT}S \qquad (3)$$

ν = the frequency of the line,

N_0 = the number of atoms in the ground level for a particular stage of ionization of the element in question,

$\tilde{\omega}_0$ = the statistical weight of the ground level,

χ_n = the excitation potential of the upper level involved in the production of the line,

T = the excitation temperature of the emitting volume,

S = the theoretical line strength.

TABLE I (*c*)

FeI—Log X'_0 values

King (I) arc' \ EP_H	3.0	3.4	3.8	4.2	4.6	5.0	5.4	5.8	6.2	6.6	7.0
2	1.90	2.25	2.61	2.98	3.36	3.78	4.21	4.64	5.09	5.58	6.08
4	2.34	2.69	3.05	3.42	3.81	4.22	4.65	5.08	5.53	6.02	6.52
6	2.60	2.95	3.31	3.68	4.07	4.48	4.91	5.34	5.79	6.28	6.78
8	2.76	3.11	3.47	3.84	4.23	4.64	5.07	5.50	5.95	6.44	6.94
10	2.92	3.27	3.63	4.00	4.39	4.80	5.23	5.66	6.11	6.60	7.10
12	3.03	3.38	3.74	4.11	4.50	4.91	5.34	5.77	6.22	6.71	7.21
15	3.17	3.52	3.88	4.25	4.64	5.05	5.48	5.91	6.36	6.85	7.35
20	3.34	3.69	4.05	4.42	4.81	5.22	5.65	6.08	6.53	7.02	7.52
25	3.50	3.85	4.21	4.58	4.97	5.38	5.81	6.24	6.69	7.18	7.68
30	3.60	3.95	4.31	4.68	5.07	5.48	5.91	6.34	6.79	7.28	7.78
35	3.71	4.06	4.42	4.79	5.18	5.59	6.02	6.45	6.90	7.39	7.89
40	3.79	4.14	4.50	4.87	5.26	5.67	6.10	6.53	6.98	7.47	7.97
45	3.86	4.21	4.57	4.94	5.33	5.74	6.17	6.60	7.05	7.54	8.04
50	3.94	4.29	4.65	5.02	5.41	5.82	6.25	6.68	7.13	7.62	8.12
60	4.04	4.39	4.75	5.12	5.51	5.92	6.35	6.78	7.23	7.72	8.22
75	4.19	4.54	4.90	5.27	5.66	6.07	6.50	6.93	7.38	7.87	8.37
100	4.37	4.72	5.08	5.45	5.84	6.25	6.68	7.11	7.56	8.05	8.55

λ 5800 – λ 6600

TABLE II (*a*)

TiI—Log X'_0 values

King (I) arc \ EP_H	2.80	3.20	3.60	4.00	4.40	4.80	5.20	5.60	6.00
3	−1.10	−0.74	−0.36	0.04	0.47	0.94	1.44	1.96	2.54
4	−0.80	−0.44	−0.06	0.34	0.77	1.24	1.74	2.26	2.84
6	−0.37	−0.01	0.37	0.77	1.20	1.67	2.17	2.69	3.27
8	−0.07	0.29	0.67	1.07	1.50	1.97	2.47	2.99	3.57
10	0.17	0.53	0.91	1.31	1.74	2.21	2.71	3.23	3.81
12	0.37	0.73	1.11	1.51	1.94	2.41	2.91	3.43	4.01
15	0.62	0.98	1.36	1.76	2.19	2.66	3.16	3.68	4.26
20	0.92	1.28	1.66	2.06	2.49	2.96	3.46	3.98	4.56
25	1.17	1.53	1.91	2.31	2.74	3.21	3.71	4.23	4.81
30	1.35	1.71	2.09	2.49	2.92	3.39	3.89	4.41	4.99
35	1.50	1.86	2.24	2.64	3.07	3.54	4.04	4.56	5.14
40	1.65	2.01	2.39	2.79	3.22	3.69	4.19	4.71	5.29
45	1.77	2.13	2.51	2.91	3.34	3.81	4.31	4.83	5.41
50	1.90	2.26	2.64	3.04	3.47	3.94	4.44	4.96	5.54
60	2.09	2.45	2.83	3.23	3.66	4.13	4.63	5.15	5.73
75	2.34	2.70	3.08	3.48	3.91	4.38	4.88	5.40	5.98
100	2.65	3.01	3.39	3.79	4.22	4.69	5.19	5.71	6.29

λ 3900 – λ 4700

Equation (3) shows that for an accurate calibration of the King intensities, one should plot Log I against (4 log ν + log $S-B$). The writer has done this using FeI values, and the results are not appreciably different from those obtained using the approximation already discussed.

The King (1, 2, 3, 4) eye estimates needed for the tables are found in the references.

TABLE II (b)

TiI—Log X'_0 VALUES

King (I) arc \ EP_H	2.50	2.90	3.20	3.60	4.00	4.40	4.80	5.20	5.60	6.00
5	−0.21	0.11	0.37	0.73	1.12	1.52	1.96	2.43	2.93	3.48
6	−0.11	0.21	0.47	0.83	1.22	1.62	2.06	2.53	3.03	3.58
8	0.18	0.50	0.76	1.12	1.51	1.91	2.35	2.82	3.32	3.87
10	0.39	0.71	0.97	1.41	1.72	2.12	2.56	3.03	3.53	4.08
12	0.57	0.89	1.15	1.59	1.90	2.30	2.74	3.21	3.71	4.26
15	0.78	1.10	1.36	1.80	2.11	2.51	2.95	3.42	3.92	4.47
20	1.05	1.37	1.63	2.07	2.38	2.78	3.22	3.69	4.19	4.74
25	1.27	1.59	1.85	2.29	2.60	3.00	3.44	3.91	4.41	4.96
30	1.44	1.76	2.02	2.46	2.77	3.17	3.61	4.08	4.58	5.13
35	1.58	1.90	2.16	2.60	2.91	3.31	3.75	4.22	4.72	5.27
40	1.70	2.02	2.28	2.72	3.03	3.43	3.87	4.34	4.84	5.39
45	1.81	2.13	2.39	2.83	3.14	3.54	3.98	4.45	4.95	5.50
50	1.92	2.24	2.50	2.94	3.25	3.65	4.09	4.56	5.06	5.61
60	2.09	2.41	2.67	3.11	3.42	3.82	4.26	4.73	5.23	5.78
75	2.31	2.63	2.89	3.33	3.64	4.04	4.48	4.95	5.45	6.00
100	2.57	2.89	3.15	3.59	3.90	4.30	4.74	5.21	5.71	6.26

λ 4800 – λ 5700

TABLE II (c)

TiI—Log X'_0 VALUES

King (I) arc \ EP_H	3.10	3.20	3.60	4.00	4.40	4.80	5.20	5.60	6.00
5	−0.04	0.03	0.40	0.77	1.13	1.50	1.87	2.23	2.60
6	0.14	0.21	0.58	0.95	1.31	1.68	2.05	2.41	2.78
8	0.35	0.42	0.79	1.16	1.52	1.89	2.26	2.62	2.99
10	0.52	0.59	0.96	1.33	1.69	2.06	2.43	2.79	3.16
12	0.66	0.73	1.10	1.47	1.83	2.20	2.57	2.93	3.30
15	0.83	0.90	1.27	1.64	2.00	2.37	2.74	3.10	3.47
20	1.05	1.12	1.49	1.86	2.22	2.59	2.96	3.32	3.69
25	1.22	1.29	1.66	2.03	2.39	2.76	3.13	3.49	3.86
30	1.35	1.42	1.79	2.16	2.52	2.89	3.26	3.62	3.99
35	1.46	1.53	1.90	2.27	2.63	3.00	3.37	3.73	4.10
40	1.56	1.63	2.00	2.37	2.73	3.10	3.47	3.83	4.20
45	1.66	1.73	2.10	2.47	2.83	3.20	3.57	3.93	4.30
50	1.74	1.81	2.18	2.55	2.91	3.28	3.65	4.01	4.38
60	1.88	1.95	2.32	2.69	3.05	3.42	3.79	4.15	4.52
75	2.05	2.12	2.49	2.86	3.22	3.59	3.96	4.32	4.69
100	2.26	2.33	2.70	3.07	3.43	3.80	4.17	4.53	4.90

λ 5800 – λ 6600

TABLE III

TiII—Log X'_0 values

King (I) arc	EP_H 3.8	4.2	4.6	5.0	5.4	5.8	6.2
2	2.56	2.92	3.27	3.63	3.98	4.33	4.69
4	2.86	3.22	3.57	3.93	4.28	4.63	4.99
6	3.02	3.39	3.74	4.10	4.45	4.80	5.16
8	3.15	3.51	3.86	4.22	4.57	4.94	5.28
10	3.25	3.61	3.96	4.32	4.67	5.02	5.38
12	3.32	3.68	4.03	4.40	4.74	5.09	5.45
15	3.42	3.78	4.13	4.50	4.84	5.19	5.55
20	3.54	3.90	4.25	4.62	4.96	5.31	5.67
25	3.64	4.00	4.35	4.72	5.06	5.41	5.77
30	3.71	4.07	4.42	4.79	5.13	5.48	5.84
35	3.77	4.13	4.48	4.85	5.19	5.54	5.90
40	3.83	4.19	4.54	4.91	5.25	5.60	5.96
45	3.87	4.23	4.58	4.95	5.29	5.64	6.00
50	3.93	4.29	4.64	5.01	5.35	5.70	6.06
60	4.00	4.36	4.71	5.08	5.42	5.77	6.13
75	4.10	4.46	4.81	5.18	5.52	5.87	6.23

$\lambda\,4000 - \lambda\,5000$

References

1. King, A. S. Astrophys. J. 37 : 239-281. 1913.
2. King, A. S. Astrophys. J. 39 : 139-165. 1914.
3. King, A. S. Astrophys. J. 56 : 318-339. 1922.
4. King, A. S. Astrophys. J. 59 : 155-176. 1924.
5. Menzel, D. H., Baker, J. G., and Goldberg, L. Astrophys. J. 87 : 81-101. 1938.
6. Russell, H. N. Proc. Nat. Acad. Sci. U.S. 11 : 314-322. 1925.
7. Russell, H. N. Proc. Nat. Acad. Sci. U.S. 11 : 322-328. 1925.
8. White, H. Phys. Rev. 44 : 753-756. 1933.
9. Wright, K. O. Astrophys. J. 99 : 249-255. 1944.

A LABORATORY STUDY OF VISIBILITY THROUGH CLOUDS[1]

By G. O. Langstroth[2], M. W. Johns[3], J. L. Wolfson[4], and H. F. Batho[5]

Abstract

Various opinions have been expressed regarding the importance of such factors as a 'diffusing effect' due to small angle scattering in determining the visual range in a cloud. If a reduction of apparent contrast and an influence on brightness level are the only important factors, conditions at the obscuration point should be described by,

$$P = CB_t10^{-\mu D}/(B_t10^{-\mu D} + B_c),$$

where B_t denotes the brightness of an object which has a contrast C with its background, B_c and μD represent respectively the cloud brightness and optical density in the line of sight, and P denotes the contrast limen value. Experiments to test this relation have been performed with an ammonium chloride smoke in a chamber 1.8 m. long. The results indicate that the equation is adequate and that factors not taken into consideration in it play a negligible role in total obscuration under laboratory conditions. The experiments were performed at various brightness levels within the 1 to 100 millilambert range.

The theory of the visual range in a cloud such as smoke or fog has received considerable attention (for a summary see reference (7)). The presence of a cloud between an observer and an object influences the brightness level at which the observer's eye must operate and results in an apparent contrast between the object and its background that is less than the actual value. Furthermore, the cloud may operate to obscure the object through additional factors such as the production by small angle scattering of apparently diffuse object boundaries. This 'diffusing effect' has been stated (1) to play an important part in obscuration but a more recent theoretical calculation (8) indicates the converse.

If the obscuring effect of a cloud is determined solely by the reduction of apparent contrast and the influence on the brightness level, it follows that at the obscuration point,

$$P = CB_t10^{-\mu D}/(B_t10^{-\mu D} + B_c), \qquad (1)$$

where B_t denotes the actual brightness of the object (assumed greater than that of the background, B_b), and B_c and μD denote respectively the cloud brightness and optical density in the line of sight. C represents the actual contrast between the object and its background, and is defined by

$$C = (B_t - B_b)/B_t. \qquad (2)$$

[1] *Manuscript received June 3, 1946.*

The experimental work on which this article is based was performed in the Department of Physics, University of Manitoba, Winnipeg, Man.

[2] *Professor of Physics, University of Alberta, Edmonton, Alta.*

[3] *Physicist, National Research Council, Chalk River Laboratory.*

[4] *Holder of a Bursary under the National Research Council of Canada.*

[5] *Associate Research Physicist, British Columbia Research Council, Vancouver, B.C.*

Mr. S. C. Fultz and Mr. Allen Kahn contributed to this work as student research assistants.

The 'contrast limen' P denotes the maximum contrast that is imperceptible to the observer. It is a function of the brightness level and the angular size of the object, and is determined by the observer's visual ability and not by any characteristic of the cloud. If the obscuring effect of a cloud is dependent on other factors Equation (1) must be extended by the addition of appropriate terms. The experiments on which this report is based were performed to ascertain whether the addition of such extra terms is necessary to describe obscuration data obtained in a smoke chamber, i.e., whether reduction of apparent contrast and influence on the brightness level are the only important factors determining the obscuring effect of a cloud under laboratory conditions.

Equation (1) may be rewritten

$$\mu D = \log\left(\frac{C - P}{P}\right) + \log(B_t/B_c). \tag{3}$$

Since P may vary, it can be expressed as $P = \phi \cdot P_0$, where ϕ is some function of the object's subtended angle and the brightness level, and P_0 denotes the value of the limen at some selected angle and brightness level. Equation (3) then reduces to

$$\mu D + \log \phi = A + \log (B_t/B_c), \tag{4}$$

where $A = \log\left(\frac{C - P}{P_0}\right)$. For brightness levels greater than about 1 mL. and subtended angles greater than 0.6°, P is 0.01 or less. Under these conditions little error is made in regarding A as a constant for objects having a contrast of 0.5 or more. A plot against log (B_t/B_c) of the optical density μD of smoke required to obscure an object (with a small correction for the log ϕ term) should on this basis yield a straight line of unit slope and constant A consistent with an acceptable value of the limen P_0. If the underlying assumptions are inadequate (i.e., if factors other than the reduction of apparent contrast and the influence on brightness level are important) departures from these characteristics may be expected. Such considerations formed the basis for the experiments.

1. Apparatus and Procedure

(a) The Smoke Chamber

The main features of the smoke chamber and its accessory apparatus are shown diagrammatically in Fig. 1. The dimensions of the chamber were 1.83 by 1.22 by 1.22 m^3. It was painted flat black inside. The observer, seated at O, made his observations through the glass window W_o. The brightness of the smoke to the observer was brought to the desired value by shining light from banks of incandescent lamps G and G' into the smoke through the glass windows W. All windows were fitted outside metal slides in the chamber walls so that they could be cleaned at any time during an experiment without disturbing the smoke. The test object T, of the form shown in Fig. 2, was enclosed in a smoke-tight box having a glass window W''. It was illuminated by shielded 6 v. battery-operated lamps L and L'. Since the test object was illuminated also by light scattered from the smoke, provi-

sion was made for measuring the illumination intensity on it by swinging photocell P into a position before section No. 1 when desired. Both the box and the window W_o were located centrally in the cross-section of the chamber. The former could be moved along the chamber axis by means of a pipe R, which also served as a conduit for connecting wires. The pipe carried a scale from which the depth of the smoke layer between the observation window W_o and the test object could be determined. The chamber was fitted with a

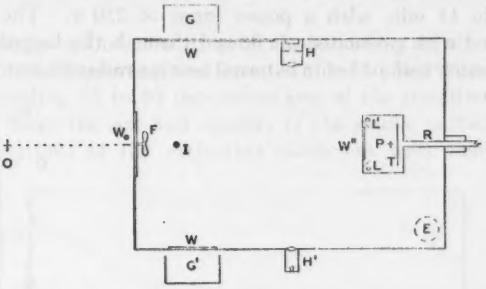

FIG. 1. *Smoke chamber and accessory apparatus; top view, approximately to scale.*

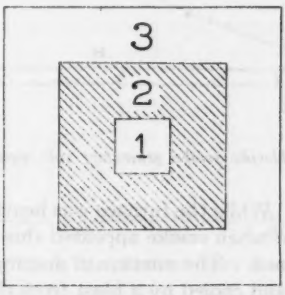

FIG. 2. *The test object. Sections Nos. 1 and 3 were white and section No. 2 was painted a uniform grey. The numerals shown were not included. The brightness contrast between sections Nos. 1 and 2 was for the most part 0.65.*

photoelectric parallel-beam device *II*, *II'* for measuring the extinction coefficient of the smoke (5). Smoke was introduced through inlet I in the bottom of the chamber and removed when desired through outlet E with the aid of a centrifugal blower. A fan F mounted just below the observation window served to dilute the smoke during production and to stir the contents of the chamber when desired.

(b) Production of Smoke

The apparatus used for producing ammonium chloride smoke is shown diagrammatically in Fig. 3. The rate of flow of air introduced at A from a compressor was controlled by valves E and C and measured by the flowmeter

F. The meter was a modification of a device (2) used for measuring the velocity of air currents not bounded by confining walls. The air was preheated to an exit temperature of 300° C. in passing through a lagged Pyrex tube *H*, 55 cm. long, containing an internal 51 ohm heating coil. To maintain this exit temperature the power dissipation was about 430 watts for an air flow of 0.36 litres per second. Ammonium chloride was placed in a Pyrex tube forming the inner walls of the 20 ohm resistance furnace *X*. Six grams was decomposed in 11 min. with a power input of 230 w. The decomposition products mixed with preheated air flowed through the lagged Pyrex tube *L*, 40 cm. long, which had a 33 ohm external heating coil sufficient to maintain the

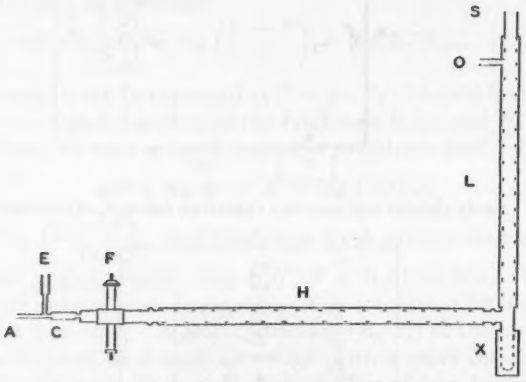

FIG. 3. *Ammonium chloride smoke generator; side view, approximately to scale.*

temperature at 300° C. While the furnace was heating, preheated air escaped through the outlet *O* but when smoke appeared this was closed and the outlet *S* into the chamber opened. The mixture of decomposition products and hot air was rapidly diluted and cooled by a blast from the fan (*F*, Fig. 1) blowing directly across the outlet *S*. The temperature rise within the chamber was about 3° C. during the production of a cloud of high optical density (e.g., 2 to 3).

(c) Procedure

In general two types of experiment, each consisting of a long series of observations, were performed. In the first type the cloud brightness B_c was maintained constant throughout the series, the test object brightness B_t (or the depth of the smoke layer before the test object) was set successively to various selected values, and the depth D of the smoke layer (or the test object brightness) was adjusted at each step until the test object was just invisible to the observer. In the second type of experiment, B_t was left unaltered throughout a series of measurements except for variations due to changes in the scattered light incident on the test object, B_c was set at various selected values and obscuration was obtained at each by adjustment of D. In judging

the obscuration point, observations were made by each of two criteria, (*a*) total disappearance, and (*b*) loss of definition. For the former, conditions were adjusted until the test object was entirely invisible; for the latter they were adjusted until section No. 1 of the object appeared as a light patch of undefined shape. While observers were perfectly adapted to the prevailing brightness level in experiments characterized by a constant B_c value, there may have been slight departures from complete adaptation in experiments in which B_c was varied.

A cycle of observations consisting of measurements at all selected values of the predetermined quantity was repeated three to five times during the life of a smoke, yielding 25 to 60 determinations of the conditions required for obscuration. Since the size and number of the smoke particles varied with time, determinations of the extinction coefficient were made at intervals

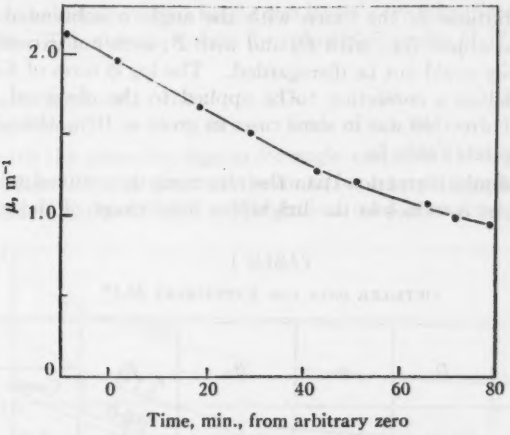

FIG. 4. *A typical extinction coefficient vs. time curve.*

and the value of μ at the time of each observation was read from a 'μ vs. time' curve plotted from the results. A typical curve is shown in Fig. 4. For the same reason, frequent adjustments were required in the illumination provided by the bank of lamps (*G*, *G'*, Fig. 1) to give the desired cloud brightness. The adjustments were made by changing the number of lamps in each bank and, in order to avoid noticeable colour differences in the illumination, only minor current variations were used. Adjustment of the test object brightness was made by varying the current through the lamps *L*, *L'* (Fig. 1).

A measurement of cloud brightness was made immediately before each obscuration determination with the aid of a flicker brightness meter (4) sighted through the observation window from a position just behind the observer. Similarly a reading of the test object brightness was made by swinging the photocell (*P*, Fig. 1) into position in front of the test object and

reading the response on a microammeter; the response was converted to terms of the brightness of section No. 1 with the aid of a calibration curve for 'response vs. brightness of section No. 1' as read with a flicker brightness meter in the absence of smoke. The brightness contrast C between sections Nos. 1 and 2 of the target was calculated from numerous flicker meter readings in the absence of smoke.

The experiments provide data on the values of μ, D, B_t, and B_c at obscuration over wide ranges of all these variables. All brightness values were based essentially on the readings of the flicker meter. The relative values of brightness (which are of primary importance in this work) are in error by not more than 3% (4). The absolute values may be more greatly in error since absolute calibration of the meter was made against a commercial illumination meter with the aid of a magnesium oxide screen.

(d) Correction for Limen Variations

Although variations in the limen with the angle α subtended by section No. 1 of the test object (i.e., with D) and with B_c were not excessive in these experiments, they could not be disregarded. The log ϕ term of Equation (4) may be regarded as a correction to be applied to the observed μD values. The size of the correction was in some cases as great as 10%, though generally it was much less (cf. Table I).

In order to obtain correction data the observers determined relative limen values for various α-values in the brightness level range of the experiments.

TABLE I

DETAILED DATA FOR EXPERIMENT 61*A**

t	μ	D	α	B_c	B_t	μD	
						Uncorr.	Corr.
6	1.87	0.50	0.92	111	5.16	0.94	0.95
12	1.76	0.76	0.82	44.1	5.23	1.34	1.37
16	1.70	0.97	0.76	12.9	5.00	1.65	1.71
22	1.60	1.28	0.69	5.20	4.95	2.05	2.18
26	1.52	1.45	0.65	2.04	3.01	2.20	2.41
32	1.46	0.72	0.84	106	6.60	1.05	1.07
36	1.40	0.93	0.77	39.8	5.60	1.30	1.35
40	1.34	1.25	0.69	12.3	5.02	1.68	1.79
46	1.26	1.45	0.65	4.86	2.05	1.83	2.01
50	1.22	1.45	0.65	2.00	1.29	1.77	1.99
55	1.15	0.89	0.78	99	7.31	1.03	1.06
59	1.11	0.98	0.76	37.8	4.00	1.09	1.14
63	1.06	1.24	0.69	13.5	2.61	1.32	1.43
77	0.95	1.16	0.72	96.2	9.5	1.10	1.16

* *B_c was set to selected values and D adjusted to obscuration at each. Corrections to the μD values have been made with the aid of Fig. 5. The time t (minutes) at which the observation was made was reckoned from an arbitrary zero set soon after the production of smoke was complete. Brightness is given in millilumberts, distance in metres, subtended angle in degrees, and extinction coefficient in metres^{-1}. The data refer to total obscuration. The observer was G.L.*

A sheet of glass was placed before the observation window at an angle of 45° to the line of sight. A large brightly illuminated white card was so placed that the observer saw its image superimposed on the test object. With no smoke in the chamber, the apparent contrast of section No. 1 was reduced until it was just imperceptible; this was done either by increasing the brightness of the veiling glare provided by the white card or by decreasing the brightness of the test object. The limen was calculated from $P = CB_t/(B_t + B')$, where B' denotes the brightness of the veiling glare. Determinations were made at various test-object-to-observer distances using total disappearance in judging the critical point. The average results obtained were as follows.

Subtended angle:	0.99°	0.84°	0.73°	0.65°
Relative limen:	1.00	1.03	1.15	1.36

The angle refers to that subtended by a side of section No. 1. Data on the relative limen values at various brightness levels were taken from the literature (3, 6, 9*, 10). The average values for subtended angles of 1° or more are as follows.

Brightness level, mL.:	100	33	10	3.3	1.0
Relative limen:	1.00	1.01	1.04	1.13	1.34

Combined with the preceding figures for angle variation these yield data for ϕ of Equation (4). P_0 was taken as the limen for a brightness level of 100 mL. and a subtended angle of 0.99°. The data as used in making the corrections

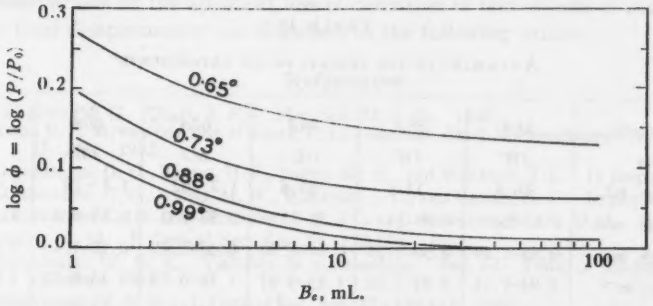

FIG. 5. *Variation of the limen with subtended angle and brightness level as used in correcting observed μD values.*

are presented in Fig. 5. The appropriate log ϕ values were added to the observed μD values. The absolute values of the limen did not enter into the considerations.

2. Results

The data for a typical experiment are given in Table I. In this experiment, as in all others, the angle subtended at the observer by a side of the illuminated

* *See paper by J. Blanchard (Phys. Rev. 11 : 81. 1918) for the brightness units appropriate to Konig and Brodhun's limen data.*

patch of smoke (i.e., the observation window) was about 15°. The surround beyond the window was relatively dark. The typical scatter encountered in these experiments is indicated by the Table I data as plotted in Fig. 6. A summary of the results of six experiments by three observers is given in Table II.

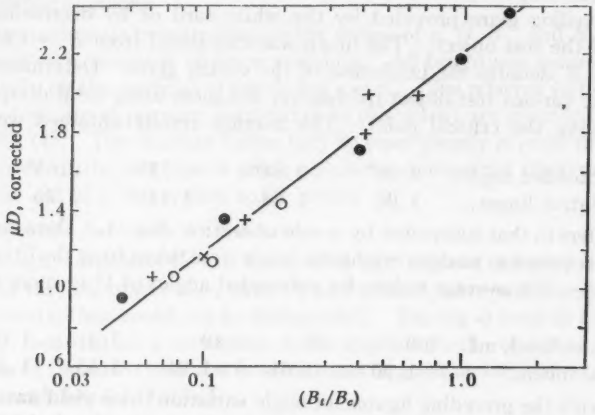

FIG. 6. *A typical plot of observed data (Expt. 61A, observer GL) illustrating the linearity of the relation, the scatter of observations, and the range covered. The points for each cycle of measurements are represented by a separate symbol.*

TABLE II

A SUMMARY OF THE RESULTS OF SIX EXPERIMENTS*

Experiment	54*A*	55*A*	56*A*	62*A*	60*A*	61*A*
Observer	*JW*	*JW*	*GL*	*MJ*	*JW*	*GL*
B_e range, mL.	16.8	17.5	20.6	1.7 –62	1.3 –76	2.0 –111
B_t range, mL.	0.50–24	0.98–34	0.77–15	0.50–7.0	0.35–6.3	1.3 –9.5
D range, m.	0.30–1.39	0.30–1.25	0.30–1.30	0.62–1.45	0.40–1.45	0.40–1.45
μ range, m^{-1}	1.93–1.15	2.07–1.05	1.85–0.97	1.70–0.72	1.48–0.77	1.91–0.95
$A(\mu D$ uncorr.)	1.76	1.82	1.79	1.81	1.69	2.04
E (μD uncorr.)	0.82	0.86	0.80	0.76	0.85	0.85
A (μD corr.)	1.93	1.94	1.90	2.04	1.80	2.22
E (μD corr.)	0.99	0.95	0.88	0.95	1.00	1.02

Averages		Uncorrected	Corrected
	A	1.82	1.99
	E	0.82	0.97

* *The data refer to total obscuration. They are described by the relation* $\mu D = A + E \log (B_t/B_e)$, *whether* μD *is corrected for limen variation with subtended angle and brightness level or not.*

3. Discussion

The experimental data exhibit a moderately large scatter as illustrated by the typical example shown in Fig. 6. The scatter is largely the result of momentary fluctuations in the visual ability of observers (cf. (3)) and can hardly be avoided in experiments of this kind. On the average, however, the relation between the various observed quantities is well represented by the data of Table II.

The range covered by the data is reasonably wide, i.e. brightness level, 1.3–111 mL.; test object brightness, 0.35–34 mL.; extinction coefficient, 0.72–2.47 m.$^{-1}$; optical density, 0.44 to 2.28; depth of smoke, 0.30 to 1.45 m. For total obscuration of the object, the results are described by

$$\mu D = 1.99 + 0.97 \log(B_t/B_e),$$

where μD has been 'corrected' by the addition of the log ϕ term to the observed values. The equation is identical in form with Equation (4) and the coefficient of the log (B_t/B_e) term is unity within the limits of experimental error. Furthermore, equating $\log(C/P_0)$ with $C = 0.65$ to the constant term one obtains a value of 0.0067 for the limen at 100 mL. and 0.99°. This is in excellent agreement with the average value for unrestricted binocular vision (0.0068) as determined in an extensive series of measurements (3). It is therefore concluded that Equation (1) is adequate and that factors such as 'diffusing effect' caused by small angle scattering play a negligible role in total obscuration under laboratory conditions.

Observations on the apparent loss of definition of test objects as contrasted with total disappearance are discussed in the following article.

References

1. Bennett, M. G. Quart. J. Roy. Met. Soc. 56 : 1-26. 1930.
2. Held, E. F. M. van der and Mulder, L. L. Koninkl. Akad. Wetenschappen Amsterdam, 35 : 267. 1932.
3. Langstroth, G. O., Batho, H. F., Johns, M. W., and Wolfson, J. L. In preparation.
4. Langstroth, G. O., Johns, M. W., Wolfson, J. L., and Batho, H. F. In preparation.
5. Langstroth, G. O. and Wolfson, J. L. Can. J. Research, A, 25 : 62-67. 1947.
6. Lowry, E. M. J. Optical Soc. Am. 21 : 132-136. 1931.
7. Middleton, W. E. K. Visibility in meteorology. 2nd ed. Univ. of Toronto Press, Toronto. 1941.
8. Middleton, W. E. K. J. Optical Soc. Am. 32 : 139-143. 1942.
9. Nutting, P. G. Bull. Bur. Standards, 5 : 261-308. 1909.
10. Stiles, W. S. and Crawford, B. H. Proc. Roy. Soc. Ser. B, 116 : 55-102. 1934.

THE RECOGNITION OF OBJECTS NEARLY OBSCURED BY A CLOUD[1]

By G. O. Langstroth[2], M. W. Johns[3], J. L. Wolfson[4], and H. F. Batho[5]

Abstract

As the apparent contrast of a square test object situated behind a smoke layer is decreased in laboratory experiments a point is reached at which the object appears as a light patch of unrecognizable shape. On decreasing the apparent contrast a little further the object becomes completely invisible. A study of the conditions under which the apparent loss of definition occurs was carried on simultaneously with the study of total obscuration described in the preceding paper. The optical density of smoke required to produce loss of definition was found to be linearly related to the logarithm of the ratio of object to cloud brightness, in close correspondence with the relation found for total obscuration. Over the range of our experiments the minimum optical density of smoke associated with loss of definition was from 12 to 23% less than that associated with total obscuration, the magnitude of the difference depending on brightness conditions. Since the phenomenon of loss of definition is observable in the presence of a veiling glare without smoke, it is probably of physiological origin.

Experiments on the total obscuration of a square test object by ammonium chloride smoke of determined extinction coefficient have been described in the preceding paper. In the experiments the layer depth or the brightness of the smoke or the illumination incident on the object was adjusted until the object became just invisible. Information was obtained on the brightness conditions and optical density of smoke required for complete obscuration over a fairly wide range of the variables involved. In the same experiments analogous data were obtained on the conditions associated with apparent loss of definition. The adjustments were made until the shape of the object became just unrecognizable although its presence was still indicated by a light patch of undefined shape. The apparatus and procedure are described in the preceding article. It is the purpose of this note to place the data on record.

Results

Data for a typical experiment are presented in Table I and Fig. 1. Table I and Fig. 6 of the preceding paper contain the corresponding data for complete obscuration in the same experiment. Table II, corresponding to Table II of the preceding paper, contains a summary of the results of seven experiments by three observers. The symbols μ, B_t, and B_c have their previous significance. D' denotes the minimum depth of smoke layer required to produce a loss of definition.

[1] *Manuscript received October 16, 1946.*

The experimental work on which this article is based was performed in the Department of Physics, University of Manitoba, Winnipeg.

[2] *Professor of Physics, University of Alberta, Edmonton, Alta.*

[3] *Physicist, National Research Council, Chalk River Laboratory.*

[4] *Holder of a Bursary under the National Research Council of Canada.*

[5] *Associate Research Physicist, British Columbia Research Council, Vancouver, B.C. Mr. S. C. Fultz and Mr. Allan Kahn contributed to this work as student research assistants.*

TABLE I

DETAILED DATA FOR EXPERIMENT 61A*

t	μ	D'	α	B_c	B_t	$\mu D'$
4	1.91	0.40	0.95	89.1	5.40	0.76
10	1.80	0.60	0.87	43.6	5.70	1.08
15	1.71	0.82	0.80	13.2	5.28	1.40
20	1.63	1.11	0.72	5.00	5.40	1.81
24	1.56	1.37	0.67	2.06	5.55	2.14
30	1.49	0.60	0.87	101	6.12	0.89
35	1.41	0.80	0.91	40.8	5.68	1.13
39	1.35	1.10	0.73	12.6	5.28	1.48
45	1.27	1.36	0.67	5.28	5.49	1.73
48	1.24	1.45	0.65	2.00	2.98	1.80
53	1.18	0.64	0.85	92.9	4.27	0.76
57	1.13	0.81	0.80	37.2	2.43	0.92
61	1.09	1.06	0.73	13.8	2.86	1.16
75	0.96	0.87	0.79	94.5	7.60	0.83

*B_c was set to selected values and D' adjusted to the point of loss of definition at each. The times t (min.) at which the observations were made were reckoned from an arbitrary zero set soon after production of smoke was complete. Brightness is given in millilamberts, distance in metres, subtended angle (α) in degrees, and extinction coefficient in metres^{-1}. The observer was G.L. The total obscuration data for this experiment are given in Table I of the preceding paper.

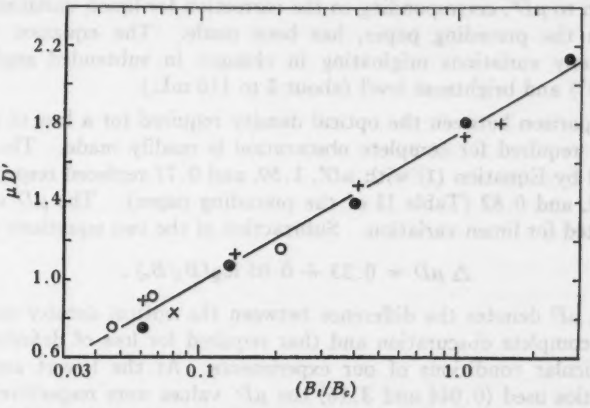

FIG. 1. *A typical plot of observed data (Expt. 61A, observer G.L.). The points for each cycle of measurements are represented by a separate symbol.*

Discussion

A plot of $\mu D'$ vs. $\log(B_t/B_c)$ shows a linear relation in all experiments. Fig. 1 provides a typical example. The scatter of plotted points is comparable to that obtained in total obscuration determinations (compare Fig. 1 with

TABLE II

A SUMMARY OF THE RESULTS OF SEVEN EXPERIMENTS*

Experiment	54A	55A	56A	62A	60A	61A	52A
Observer	JW	JW	GL	MJ	JW	GL	GL
B_o range, mL.	16.8	17.5	20.6	1.7–62	1.3–76	2.0–111	12.3
B_t range, mL.	0.50–24	0.98–34	0.77–15	0.50–7.0	0.35–6.3	1.3–9.5	0.54–34
D' range, m.	0.30–1.39	0.30–1.25	0.30–1.30	0.62–1.45	0.40–1.45	0.40–1.45	0.30–1.36
μ range, m.$^{-1}$	1.93–1.15	2.07–1.05	1.85–0.97	1.70–0.72	1.48–0.77	1.91–0.95	2.47–1.45
A'	1.55	1.55	1.62	1.56	1.37	1.77	1.71
E'	0.77	0.83	0.80	0.70	0.71	0.77	0.78
Averages	$A' = 1.59$					$E' = 0.77$	

* *The data plotted for each experiment were found to be well described by the relation* $\mu D' = A' + E' \log(B_t/B_o)$; *see Fig. 1. The data on total obscuration for the above experiments may be found in Table II of the preceding paper.*

Fig. 6 of the preceding paper). Using the average results given in Table II, the minimum optical density required to produce a loss of definition is described by

$$\mu D' = 1.59 + 0.77 \log (B_t/B_o) . \quad (1)$$

This equation is simply a statement of average experimental results; no correction to $\mu D'$, corresponding to the correction for limen variation applied to μD in the preceding paper, has been made. The equation therefore includes any variations originating in changes in subtended angle (about 0.6° to 1°) and brightness level (about 2 to 110 mL.).

A comparison between the optical density required for a loss of definition and that required for complete obscuration is readily made. The latter is described by Equation (1) with $\mu D'$, 1.59, and 0.77 replaced respectively by μD, 1.82, and 0.82 (Table II of the preceding paper). The μD values are uncorrected for limen variation. Subtraction of the two equations yields,

$$\triangle \mu D = 0.23 + 0.05 \log(B_t/B_o) , \quad (2)$$

where $\triangle \mu D$ denotes the difference between the optical density required to produce complete obscuration and that required for loss of definition under the particular conditions of our experiments. At the lowest and highest B_t/B_o ratios used (0.044 and 3.16) the μD values were respectively 23 and 12% less than the μD values. Any effect produced by variation in subtended angle of the test object is contained implicitly in Equation (2).

As described in the preceding paper, corrections for limen variations with subtended angle and brightness level were applied to the total obscuration data. No corresponding corrections have been attempted for the loss of definition data because of the lack of appropriate information. In determining limen values with the aid of a veiling glare in the absence of smoke, however, it was noted that loss of definition preceded total disappearance as the

apparent contrast of the object was gradually decreased. The corners of the square test object became indistinct so that it might easily have been confused with a disk although its presence was not in doubt. Since the phenomenon of loss of definition was observed in the absence of smoke, it is considered to be of physiological origin; it is probably not connected with any objective factor such as a diffusing effect caused by the smoke.

A NOTE ON THE DETERMINATION OF THE EXTINCTION COEFFICIENT OF AEROSOLS[1]

By G. O. Langstroth[2] and J. L. Wolfson[3]

Abstract

Difficulties were encountered in smoke chamber experiments in obtaining reliable extinction coefficient data by methods based on brightness measurements of bright and 'black' surfaces seen through the smoke. These difficulties led to an investigation of the reliability of a commonly used method employing a parallel light beam and a photoelectric cell. The results indicate that the method is capable of yielding extinction coefficient data with an accuracy of 1 to 2% under the conditions of our experiments.

A surface of brightness B_0 seen through a smoke layer of depth d and extinction coefficient μ has an apparent brightness B given by

$$B = B_e + B_0 10^{-\mu d},$$

where B_e denotes the smoke brightness in the line of sight. The extinction coefficient is described by

$$\mu = 1/d \,.\, \log(B_0/(B - B_e)),$$

and can be determined if the other quantities are measured. An attempt to use this method in smoke chamber experiments with smokes having coefficients in the range 0.7 to 2.5 m.$^{-1}$ proved unsuccessful. The 20 by 20 cm.^{2} surface was located about 20 cm. behind the glass window of a small smoke-tight box that could be moved along the chamber axis to alter the d-value, and was illuminated by shielded lamps within the box. The smoke chamber is described elsewhere (1). Brightness measurements were made with a flicker brightness meter (2). Determinations of B_e made with the meter sighted just beyond the boundary of the surface led to μ-values which depended on B_0 and were obviously incorrect. When the B_e determinations were made with the meter sighted on the opening of a 4 cm. diameter tube located near the centre of the surface and serving as a 'black' body, the resulting μ-values were acceptable in this respect. They were however 20 to 30% lower than those expected from the slope of curves for 'log B_0 vs. layer depth at obscuration' as obtained with a constant veiling glare produced by the reflection of an illuminated white card in a 45° glass sheet in front of the observer. These difficulties were associated with an inability to make

[1] *Manuscript received June 3, 1946.*

The experimental work on which this article is based was performed in the Department of Physics, University of Manitoba, Winnipeg, Man.

[2] *Professor of Physics, University of Alberta, Edmonton, Alta.*

[3] *Holder of a Bursary under the National Research Council of Canada. Mr. S. C. Fultz and Mr. Allan Kahn contributed to this work as student research assistants.*

appropriate determinations of cloud brightness, and led to an investigation of a method employing a parallel beam of light and a photocell. The investigation forms the basis of this report.

1. The Nature of the Experiments

(*a*) *The photoelectric parallel-beam method.*—This method, which is not original with us, has been used in several laboratories, but we do not know the name of the originator. The experimental arrangement used by us is shown diagrammatically in Fig. 1. A collimating and a condensing lens (L and L', focal length 10 cm.) were placed at the opposite sides of the smoke chamber, a distance of 1.30 m. apart. A 21 cp. automobile lamp placed at the principal focus of the lens L and operated at constant voltage served as the light source S. A screen D containing a small opening was placed at the principal focus of the lens L'. The purpose of the screen was to prevent as much of the scattered light as possible from reaching the vacuum photocell P while permitting the directly transmitted light forming the image of the filament of S to do so. The relation between the amplified photoelectric current and the light energy incident on the cell was determined over the required range with the aid of large Nicol prisms inserted between L and L'. Denoting the light energy incident on the cell in the presence and in the absence of smoke by I and I_0, respectively, the extinction coefficient of the smoke was calculated from $\mu = \log(I_0/I)/1.30$.

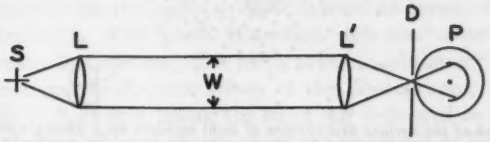

FIG. 1. *Diagram of the experimental arrangement for the parallel-beam method of extinction coefficient measurement.*

(*b*) *Dependence of μ on the width W of the collimated light beam.*—In order for the method to prove satisfactory the contribution of directly transmitted light to the energy incident on the photocell must predominate. Compared to it the contribution of light that has undergone scattering within the beam, or has been scattered back from regions outside, must be negligibly small. The directly transmitted light forms an image of the lamp filament in the plane of the screen but the scattered light is incapable of doing so. The contribution of scattered light to the total incident on the photocell is expected to depend on the beam width W (Fig. 1), approaching zero for an infinitely narrow beam. An observed dependence of μ on beam width might therefore be taken as an indication that scattered light cannot be neglected. Experiments to test this point were performed with the aid of diaphragms of various

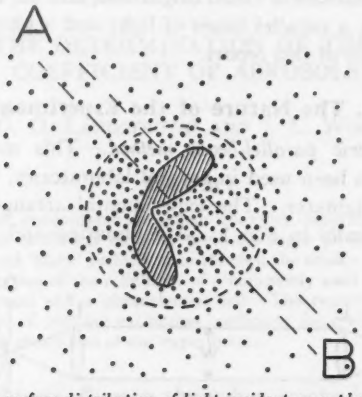

FIG. 2. *Sketch of the surface distribution of light incident on a photographic plate placed in the plane of the screen D (Fig. 1). The image formed by directly transmitted light is shaded, and the incidence of scattered light is indicated by the dotted area. The dashed circle indicates the position of the opening in the screen. The plate was photometered along the band AB.*

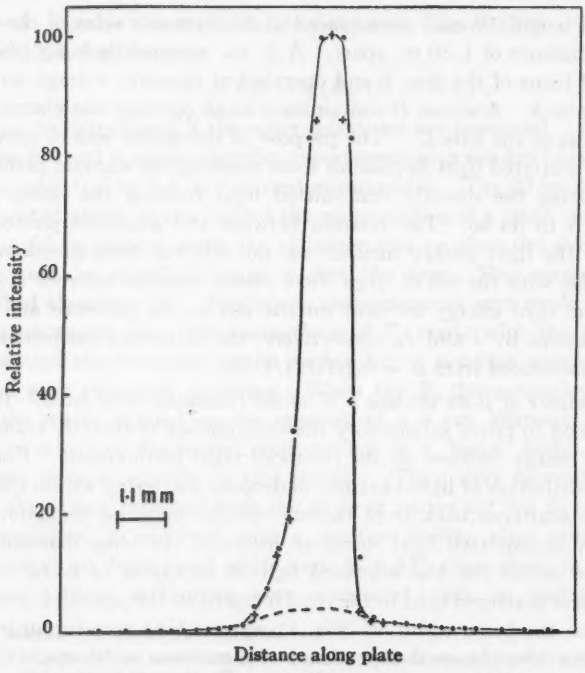

FIG. 3. *Intensity contour obtained by photometering two photographic plates. Outside the main image the intensity is low, and measurements indicated elsewhere by + have been omitted to avoid confusion. The unplotted points fall closely along those plotted. The dashed line suggests an upper limit for the intensity of scattered light in the area occupied by the filament image.*

sizes inserted at the collimating lens. Typical results are given in Table I of Section 2.

(*c*) *Estimation of an upper limit for the contribution of scattered light.*—In order to obtain an estimate of the relative energies associated with directly transmitted and scattered light admitted to the photocell, the screen *D* (Fig. 1) was replaced by a photographic plate. A short exposure was made in the early stages of a smoke using a beam width of 3.9 cm. Calibration marks were placed on the plate with the aid of an adjustable high speed sector and a light source of appropriate energy–wave-length distribution. These permitted photographic densities on the plate to be converted to terms of the relative light energies incident. The plate (Eastman 40) was somewhat underdeveloped to produce low contrast, care being taken to minimize the Eberhardt effect. Microphotometric determinations of the photographic density were made at intervals of 0.28 mm. along the band *AB* indicated in Fig. 2. The determined distribution of light energy along the band *AB* of Fig. 2 is shown in Fig. 3 of Section 2.

(*d*) *The dependence of μ on the angle of divergence of a non-parallel beam.*—If permissible, the use of a somewhat divergent beam of light has certain advantages since the adjustments are less critical and the apparatus consequently more rugged. Series of measurements of μ were made with beams of various divergence. The divergence was controlled by adjusting the distance between the light source and the collimating lens. Typical results are given in Table II of Section 2.

2. Results

TABLE I

A COMPARISON OF THE μ-VALUES OBTAINED WITH PARALLEL BEAMS OF VARIOUS WIDTHS IN TYPICAL EXPERIMENTS*

Experiment	t	μ-Values for beam widths of				
		3.94	3.30	2.06	1.31	0.88
47*A*	6– 8.5	1.82	1.80	1.90	1.95	1.84
	16– 20	1.87	1.85	1.90	1.93	1.88
	52– 56	1.74	1.72	1.79	1.75	1.68
	71– 75	1.67	1.64	1.69	1.64	1.65
	106–110	1.48	1.45	1.49	1.50	1.47
49*A*	12– 15	2.39	2.38	2.38	2.33	—
	65– 68	1.77	1.76	1.76	1.76	—
48*A*	3.5–6	2.81	2.88	2.95	2.88	—
	40– 42.5	2.80	2.86	2.87	2.85	—
	111–112.5	2.37	2.42	2.45	2.43	—

* *Beam width is given in cm., and t denotes the time interval (min.) in which the observations were made as reckoned from an arbitrary zero set soon after complete generation of ammonium chloride smoke.*

TABLE II

A COMPARISON OF μ-VALUES OBTAINED WITH BEAMS OF VARIOUS ANGLES OF DIVERGENCE*

t	μ-Values for divergence angles (degrees) of								
	0.0	2.6	4.6	7.6	10.0	15.6	20.0	24.0	30.0
13–19	1.85	1.85	1.84	1.71	1.67	1.63	1.59	1.56	1.54
30–36	1.63	1.64	1.62	1.55	1.53	1.50	1.45	1.44	1.43
53–59	1.47	1.47	1.43	1.34	1.31	1.27	1.22	1.21	1.19

** The angle θ referred to is the plane angle at the apex of the cone formed by projecting backward the boundaries of the ray bundle between the collimating and condensing lenses. The time interval t has the same significance as in Table I. For θ values of 4.6° or less the collimating lens was diaphragmed down to a diameter of 1.31 cm.; for the others the diameter of the diaphragm was 3.94 cm.*

3. Discussion

The particulate characteristics of a smoke change with time. In the experiments each group of measurements to be compared was made as rapidly as possible to minimize this factor. Examination of the decrease in extinction coefficient with time for a given beam width (Table I) indicates that changes in smoke characteristics during the time interval required for a group of comparative determinations caused a decrease of not more than 0.01 to 0.02 in the extinction coefficient value.

The results of Table I show no systematic variation of the determined extinction coefficient value with beam width. The average deviation of individual μ-values from the means for the groups is 1.2%. This evidence supports the view that the contribution of scattered light to the energy incident on the photocell is negligible in the parallel-beam method.

The contour of Fig. 3 indicates the surface distribution of energy incident on the screen before the photocell. A probable upper limit for the scattered energy in the region of the filament image is indicated by the dashed line in the figure. A comparison of the energies of scattered and directly transmitted light admitted to the photocell was made by integration under the respective contours over the area of the screen opening. The result indicates that the former was less than 7% of the latter. This value is an upper limit. The occurrence of halation and diffusion of light in traversing the emulsion are factors that would influence the extrapolation of the scattered light contour toward spuriously high values, and the use of a colour blind emulsion probably favoured the scattered at the expense of the transmitted light. The Eberhardt effect would operate in the opposite direction, but no evidence of its presence is detectable in the contour of Fig. 3. At worst, a 7% error in transmitted energy introduces an error of 1% in an extinction coefficient of 2.00 and an error of 2% in a coefficient of 1.00. The result indicates that the parallel-beam method is capable of yielding accurate values for the extinction coefficient.

The results quoted in Table II show that it is not important to use a strictly parallel beam under the conditions of these experiments. Divergences of as much as 5° appear permissible.

Extinction coefficients measured by the parallel-beam method were found to be about 20% higher than those determined with the aid of a brightness meter, an illuminated surface, and a 'black' body as described in the introduction. As mentioned there, this finding is in accord with the results of obscuration data.

References

1. LANGSTROTH, G. O., JOHNS, M. W., WOLFSON, J. L., and BATHO, H. F. Can. J. Research, A, 25 : 49-57. 1947.
2. LANGSTROTH, G. O., JOHNS, M. W., WOLFSON, J. L., and BATHO, H. F. In preparation.

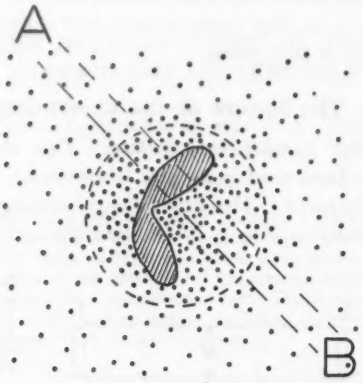

FIG. 2. *Sketch of the surface distribution of light incident on a photographic plate placed in the plane of the screen D (Fig. 1). The image formed by directly transmitted light is shaded, and the incidence of scattered light is indicated by the dotted area. The dashed circle indicates the position of the opening in the screen. The plate was photometered along the band AB.*

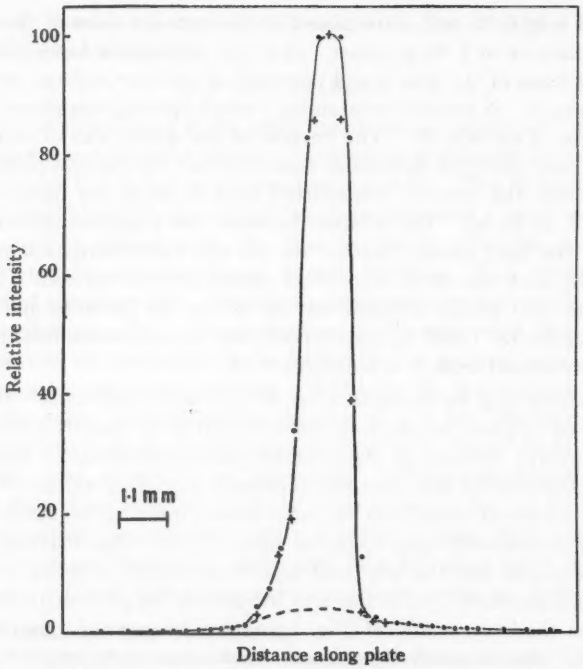

FIG. 3. *Intensity contour obtained by photometering two photographic plates. Outside the main image the intensity is low, and measurements indicated elsewhere by + have been omitted to avoid confusion. The unplotted points fall closely along those plotted. The dashed line suggests an upper limit for the intensity of scattered light in the area occupied by the filament image.*

sizes inserted at the collimating lens. Typical results are given in Table I of Section 2.

(*c*) *Estimation of an upper limit for the contribution of scattered light.*—In order to obtain an estimate of the relative energies associated with directly transmitted and scattered light admitted to the photocell, the screen *D* (Fig. 1) was replaced by a photographic plate. A short exposure was made in the early stages of a smoke using a beam width of 3.9 cm. Calibration marks were placed on the plate with the aid of an adjustable high speed sector and a light source of appropriate energy–wave-length distribution. These permitted photographic densities on the plate to be converted to terms of the relative light energies incident. The plate (Eastman 40) was somewhat underdeveloped to produce low contrast, care being taken to minimize the Eberhardt effect. Microphotometric determinations of the photographic density were made at intervals of 0.28 mm. along the band *AB* indicated in Fig. 2. The determined distribution of light energy along the band *AB* of Fig. 2 is shown in Fig. 3 of Section 2.

(*d*) *The dependence of μ on the angle of divergence of a non-parallel beam.*—If permissible, the use of a somewhat divergent beam of light has certain advantages since the adjustments are less critical and the apparatus consequently more rugged. Series of measurements of μ were made with beams of various divergence. The divergence was controlled by adjusting the distance between the light source and the collimating lens. Typical results are given in Table II of Section 2.

2. Results

TABLE I

A COMPARISON OF THE μ-VALUES OBTAINED WITH PARALLEL BEAMS OF VARIOUS WIDTHS IN TYPICAL EXPERIMENTS*

Experiment	t	μ-Values for beam widths of				
		3.94	3.30	2.06	1.31	0.88
47*A*	6– 8.5	1.82	1.80	1.90	1.95	1.84
	16– 20	1.87	1.85	1.90	1.93	1.88
	52– 56	1.74	1.72	1.79	1.75	1.68
	71– 75	1.67	1.64	1.69	1.64	1.65
	106–110	1.48	1.45	1.49	1.50	1.47
49*A*	12– 15	2.39	2.38	2.38	2.33	—
	65– 68	1.77	1.76	1.76	1.76	—
48*A*	3.5–6	2.81	2.88	2.95	2.88	—
	40– 42.5	2.80	2.86	2.87	2.85	—
	111–112.5	2.37	2.42	2.45	2.43	—

* *Beam width is given in cm., and t denotes the time interval (min.) in which the observations were made as reckoned from an arbitrary zero set soon after complete generation of ammonium chloride smoke.*

TABLE II

A COMPARISON OF μ-VALUES OBTAINED WITH BEAMS OF VARIOUS ANGLES OF DIVERGENCE*

t	μ-Values for divergence angles (degrees) of								
	0.0	2.6	4.6	7.6	10.0	15.6	20.0	24.0	30.0
13–19	1.85	1.85	1.84	1.71	1.67	1.63	1.59	1.56	1.54
30–36	1.63	1.64	1.62	1.55	1.53	1.50	1.45	1.44	1.43
53–59	1.47	1.47	1.43	1.34	1.31	1.27	1.22	1.21	1.19

** The angle θ referred to is the plane angle at the apex of the cone formed by projecting backward the boundaries of the ray bundle between the collimating and condensing lenses. The time interval t has the same significance as in Table I. For θ values of 4.6° or less the collimating lens was diaphragmed down to a diameter of 1.31 cm.; for the others the diameter of the diaphragm was 3.94 cm.*

3. Discussion

The particulate characteristics of a smoke change with time. In the experiments each group of measurements to be compared was made as rapidly as possible to minimize this factor. Examination of the decrease in extinction coefficient with time for a given beam width (Table I) indicates that changes in smoke characteristics during the time interval required for a group of comparative determinations caused a decrease of not more than 0.01 to 0.02 in the extinction coefficient value.

The results of Table I show no systematic variation of the determined extinction coefficient value with beam width. The average deviation of individual μ-values from the means for the groups is 1.2%. This evidence supports the view that the contribution of scattered light to the energy incident on the photocell is negligible in the parallel-beam method.

The contour of Fig. 3 indicates the surface distribution of energy incident on the screen before the photocell. A probable upper limit for the scattered energy in the region of the filament image is indicated by the dashed line in the figure. A comparison of the energies of scattered and directly transmitted light admitted to the photocell was made by integration under the respective contours over the area of the screen opening. The result indicates that the former was less than 7% of the latter. This value is an upper limit. The occurrence of halation and diffusion of light in traversing the emulsion are factors that would influence the extrapolation of the scattered light contour toward spuriously high values, and the use of a colour blind emulsion probably favoured the scattered at the expense of the transmitted light. The Eberhardt effect would operate in the opposite direction, but no evidence of its presence is detectable in the contour of Fig. 3. At worst, a 7% error in transmitted energy introduces an error of 1% in an extinction coefficient of 2.00 and an error of 2% in a coefficient of 1.00. The result indicates that the parallel-beam method is capable of yielding accurate values for the extinction coefficient.

The results quoted in Table II show that it is not important to use a strictly parallel beam under the conditions of these experiments. Divergences of as much as 5° appear permissible.

Extinction coefficients measured by the parallel-beam method were found to be about 20% higher than those determined with the aid of a brightness meter, an illuminated surface, and a 'black' body as described in the introduction. As mentioned there, this finding is in accord with the results of obscuration data.

References

1. LANGSTROTH, G. O., JOHNS, M. W., WOLFSON, J. L., and BATHO, H. F. Can. J. Research, A, 25 : 49-57. 1947.
2. LANGSTROTH, G. O., JOHNS, M. W., WOLFSON, J. L., and BATHO, H. F. In preparation.

A NOTE ON PHASE CORRECTION IN ELECTRICAL DELAY NETWORKS[1]

By Alex. J. Ferguson[2]

Abstract

The standard method of correcting the phase characteristic of low-pass networks by introducing mutual inductance between the coils is extended. By means of mutual inductance between the coils and a capacity across them, it is possible to eliminate the third and fifth order terms in the variation of the phase shift with frequency. The relation required between the circuit constants for this result is given, and is found to be very simple.

There are a number of systems that may be used to provide a small delay for a video signal. These may be divided roughly into two categories; those with distributed constants, and those with lumped constants. In the first category are concentric lines with coiled inner conductors and the 'condensed cables' suggested by Kallmann (2). These are simple devices, fairly readily constructed, and they provide a reasonably good solution to the problem. Their performance is not perfect—they suffer phase defects at frequencies for which the wave-length along the structure is comparable with its diameter. In the second category are wave filters and standard artificial lines. It is with a network of this type that this report is concerned. Holcomb (1) has described an elaborate bridged-T delay network with excellent phase characteristics, which, however, is much too complicated for high frequency ranges.

It is well known (3, p. 245) that the phase characteristic of a simple low-pass filter can be improved by introducing mutual inductance between adjacent coils as shown in Fig. 1. Let θ be the phase shift of a single section and ω the radian frequency. θ is an odd function of ω, so that if θ is expanded in a Maclaurin series, we obtain

$$\theta = \theta_1 \omega + \theta_3 \omega^3 + \theta_5 \omega^5 + \ldots \ldots \quad (1)$$

$\theta_1, \theta_3, \theta_5, \ldots$ are the Maclaurin coefficients and are functions of the network parameters. We may choose the mutual inductance so that θ_3 vanishes, removing the third order term in ω. The condition for this is*

$$L - 6M = 0 \quad (2)$$

Some attention must be given the sign of M. Equation (2) implies that the coils are series-aiding.

[1] *Manuscript received June 7, 1946.*

Contribution from the Radio Branch, Division of Physics and Electrical Engineering, National Research Laboratories, Ottawa, Canada. Issued as N.R.C. No. 1474.

[2] *Physicist.*

* *The network is essentially equivalent to a series m-derived filter with $m = \sqrt{1.5}$. Starr recommends $m = \sqrt{2}$, which is over-corrected in the sense taken here. It should be noted that a chain of m-type sections would produce a network with the inductances divided in halves in the manner suggested at the end of the paper.*

It will be shown how to introduce another circuit parameter to obtain yet another order of phase correction, the word 'correction' here having the significance used above, i.e., the removal of successive non-linear terms of Equation (1). The circuit is that of Fig. 2, the added element being a condenser C_1 across the inductance L. C_1 and M may be chosen so that the θ_3 and θ_5 for this circuit both vanish. The required conditions reduce to a very simple form, namely

$$L - 6.439\, M = 0 \tag{3}$$

$$C_2 - 28.439\, C_1 = 0 \tag{4}$$

Here again it is found that the coils are series-aiding.

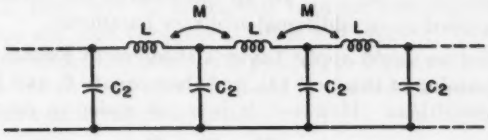

FIG. 1. *Simple low-pass filter delay network with mutual inductance for phase correction.*

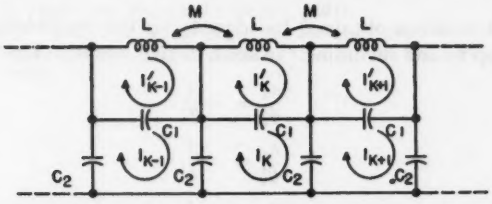

FIG. 2. *Low-pass delay network using both mutual inductance and a capacity, C_1, for phase correction.*

This result is obtained by laborious but straightforward algebra. Only an outline of the calculation will be given. The network equations are:

$$I_k\left(\frac{2}{j\omega C_2} + \frac{1}{j\omega C_1}\right) - \frac{I'_k}{j\omega C_1} - \frac{1}{j\omega C_2}(I_{k-1} + I_{k+1}) = 0\,. \tag{5}$$

$$I'_k\left(j\omega L + \frac{1}{j\omega C_1}\right) - \frac{I_k}{j\omega C_1} + j\omega M\,(I'_{k-1} + I'_{k+1}) = 0\,. \tag{6}$$

If we put

$$I_k = Ae^{k\gamma}$$
$$I'_k = A'e^{k\gamma}\,,$$

where A and A' are arbitrary constants and γ the propagation constant, then the consistency of Equations (5) and (6) requires that

$$\cosh^2\gamma - \frac{1}{2}\left\{\frac{C_2}{C_1} + 2 - \frac{L}{M} + \frac{1}{\omega^2 MC_1}\right\}\cosh\gamma$$
$$- \frac{1}{4}\left\{\frac{L}{M}\left(\frac{C_2}{C_1} + 2\right) - \frac{2}{\omega^2 MC_1}\right\} = 0\,. \tag{7}$$

Equation (7) determines the propagation constant γ.

As there are two solutions for cosh γ, there are two modes of transmission. One of these is rapidly attenuated at all frequencies and does not concern us. The other mode has a low-pass filter type of behaviour that is susceptible of the improvement obtained by choosing the circuit constants properly.

In the pass band, γ is purely imaginary and equal to $j\theta$. The solution of Equation (7) then gives us cos θ. This solution may be expanded as a Maclaurin series in ω:

$$\cos\theta = 1 + a_2\omega^2 + a_4\omega^4 + a_6\omega^6 + \ldots\ldots$$

$$= 1 + \frac{a_2}{\theta_1^2}(\theta_1\omega)^2 + \frac{a_4}{\theta_1^4}(\theta_1\omega)^4 + \frac{a_6}{\theta_1^6}(\theta_1\omega)^6 + \ldots. \tag{8}$$

The coefficients a_2, a_4, a_6, . . . are all functions of the network parameters. θ_1 may be regarded as an additional arbitrary parameter.

At this point we could apply Taylor's theorem to Equation (7) or (8) to obtain an expansion of the form (1), and then equate θ_3 and θ_5 to zero to get our desired conditions. However, it is much easier to proceed as follows. We have

$$\cos\theta = 1 - \frac{\theta^2}{2!} + \frac{\theta^4}{4!} - \frac{\theta^6}{6!} + \ldots. \tag{9}$$

The required result is obtained by identifying the coefficients of Equations (8) and (9) up to and including the sixth degree terms. That is, we put

$$\frac{a_2}{\theta_1^2} = -\frac{1}{2!}$$

$$\frac{a_4}{\theta_1^4} = \frac{1}{4!}$$

$$\frac{a_6}{\theta_1^6} = -\frac{1}{6!}.$$

Eliminating θ_1 between these equations gives us two equations for the circuit parameters, M and C_1. These can be reduced to

$$L = 6.439\,M$$

$$C_2 = 28.439\,C_1$$

that is, Equations (3) and (4).

Turning to other important constants of the circuit, we may readily find that the cut-off frequency is

$$\omega_0 = \frac{2}{\sqrt{(L - 2M)(C_2 + 4C_1)}}.$$

The question of the characteristic impedance or the proper terminating impedance is more difficult. If the mutually coupled coils be replaced by their T equivalents, it will be seen that the ladder becomes not a chain of four-terminal networks, but of six-terminal networks. It is this fact that is responsible for the two modes of propagation. Such a network requires two characteristic impedances.

In a practical case the line will probably be broken off at one of the junction points as they appear in Fig. 2. This procedure destroys the six-terminal character of the last section, but there does not seem to be any good reason for attempting to preserve it. The terminating admittance which will remove the reflected propagated wave for such an arrangement can be calculated. The result appears to be complicated—it has not been carried through in any case. It will undoubtedly be mainly resistive, of a value close to $\sqrt{L/C_2}$. Experience with networks with a cut-off frequency of 5 megacycles per second indicates that the results are uncritical to the termination.

It has been assumed that there is no mutual inductance between any pairs of coils except adjacent ones. If the coils are mounted coaxially, this will not be true, i.e. there will be interaction between non-adjacent coils. The effect of this has not been considered, but it will probably be small. If any concern were felt about this point, it is possible to divide each coil in half and then to arrange the parts so that a half-coil in one section interacts only with the adjacent half-coil in the next section.

References

1 HOLCOMB, R. T. Bell Labs. Record, 9 : 229-232. 1931.
2. KALLMANN, H. E. Proc. Inst. Radio Engrs. 28 : 302-310. 1940.
3. STARR, A. T. Electric circuits and wave filters. 2nd ed. Sir Isaac Pitman & Sons, Ltd., London. 1938.

CANADIAN JOURNAL OF RESEARCH

Notes on the Preparation of Copy

GENERAL:—Manuscripts should be typewritten, double spaced, and the **original and at least one extra** copy submitted. Style, arrangement, spelling, and abbreviations should conform to the usage of this Journal. Names of all simple compounds, rather than their formulae, should be used in the text. Greek letters or unusual signs should be written plainly or explained by marginal notes. Superscripts and subscripts must be legible and carefully placed. Manuscripts should be carefully checked before being submitted, to reduce the need for changes after the type has been set. **All pages, whether text, figures, or tables, should be numbered.**

ABSTRACT:—**An abstract of not more than about 200 words, indicating the scope of the work and the principal findings, is required.**

ILLUSTRATIONS:—

(i) *Line Drawings:*—All lines should be of sufficient thickness to reproduce well. Drawings should be carefully made with India ink on white drawing paper, blue tracing linen, or co-ordinate paper **ruled in blue only**; any co-ordinate lines that are to appear in the reproduction should be ruled in black ink. Paper ruled in **green, yellow, or red should not be used** unless it is desired to have all the co-ordinate lines show. Lettering and numerals should be neatly done in India ink preferably with a stencil (**do not use typewriting**) and be of such size that they will be legible and not less than one millimetre in height when reproduced in a cut three inches wide. All experimental points should be carefully drawn with instruments. Illustrations need not be more than two or three times the size of the desired reproduction, but the ratio of height to width should conform with that of the type page. **The original drawings and one set of small but clear photographic copies are to be submitted.**

(ii) *Photographs:*—Prints should be made on glossy paper, with strong contrasts; they should be trimmed to remove all extraneous material so that essential features only are shown. Photographs should be submitted **in duplicate;** if they are to be reproduced in groups, one set should be so arranged and mounted on cardboard with rubber cement; the duplicate set should be unmounted.

(iii) *General:*—**The author's name, title of paper, and figure number should be written on the back of each illustration.** Captions should not be written on the illustrations, but typed on a separate page of the manuscript. All figures (including each figure of the plates) should be numbered consecutively from 1 up (arabic numerals). **Each figure should be referred to in the text.**

TABLES:—Titles should be given for all tables, which should be numbered in Roman numerals. Column heads should be brief and textual matter in tables confined to a minimum. **Each table should be referred to in the text.**

REFERENCES:—**These should be listed alphabetically by authors' names, numbered in that order, and placed at the end of the paper.** The form of literature citation should be that used in this Journal. **Titles of papers should not be given in references listed in Sections A, B, E, and F, but must be given in references listed in Sections C and D. All citations should be checked with the original articles.** Each citation should be referred to in the text by means of the key number; in Sections C and D the author's name and the date of publication may be included with the key number if **desired.**

The *Canadian Journal of Research* conforms in general with the practice outlined in the *Canadian Government Editorial Style Manual*, published by the Department of Public Printing and Stationery, Ottawa.

Reprints

Fifty reprints of each paper are supplied free. Additional reprints, if required will be supplied according to a prescribed schedule of charges.